THE VERTICAL TEMPERATURE STRUCTURE OF THE MID-LATITUDE TROPOSPHERE: A SIMPLE MODEL

by

JEFFREY ALAN STEPHENSON

B.A., Pomona College

(1973)

SUBMITTED IN PARTIAL FULFILLMENT

OF THE REQUIREMENTS FOR THE

DEGREE OF

MASTER OF SCIENCE

at the

MASSACHUSETTS INSTITUTE OF TECHNOLOGY

JULY, 1977

Signature of Author . . . . . .
Department of Meteorology, July 1977

Certified by . . . . . .
Thesis Supervisor

Accepted by . . . . . .
Chairman, Department Committee

THE VERTICAL TEMPERATURE STRUCTURE OF THE MID-LATITUDE TROPOSPHERE: A SIMPLE MODEL

by
Jeffrey Alan Stephenson

Submitted to the Department of Meteorology on
July 29, 1977 in partial fulfillment of the requirements
for the degree of Master of Science

ABSTRACT

A simple one dimensional model is developed to account for the observed vertical temperature structure of the mid-latitude troposphere. The model includes radiative heat fluxes through a simple linearized law and convection via a convective adjustment. The novel feature of the model is the inclusion of the vertical heat fluxes due to baroclinic eddies.

Given an initial vertical temperature profile, the structure of the eddies is calculated from linear stability theory and the amplitude is determined from a finite amplitude equilibration condition. The vertical heat flux due to the eddies is then computed and this flux is used, with the radiative flux, to integrate the thermal equation forward in time to obtain a new temperature profile. A convective adjustment is performed if necessary, and the process is continued until an equilibrium temperature profile is reached.

The model is first integrated without the eddy heat fluxes to obtain a radiative-convective temperature profile. This serves as both a starting point for the radiative-dynamical calculations and as a basis for comparison of the results of the radiative-dynamical calculations. Radiative dynamical equilibrium (RDE) profiles are then calculated for baroclinic waves of zonal wavenumber 3, 6, and 9. The RDE profiles for wavenumbers 3 and 6 do not differ significantly from the radiative-convective equilibrium (RCE) state; in particular the profiles still have fairly deep convective regions at the bottom of the atmosphere. The RDE profile for wavenumber 9, however, is stable all the way to the ground and, except for being somewhat too cold, is remarkably similar to the observed temperature profile at 45° N . It is thus suggested that the small scale cyclone waves observed in the atmosphere are responsible for maintaining the observed static stability.

Thesis supervisor: Peter H. Stone
Title: Professor of Meteorology

ACKNOWLEDGEMENTS

I would like to express my thanks to my thesis advisor, Professor Peter H. Stone, whose advice and comments concerning this thesis have been invaluable and from whom I have learned what I know of the philosophy of atmospheric modelling. Appreciation is also due to Professor Jule G. Charney from whom I have learned something of geophysical fluid dynamics and whose intuitive understanding of physical processes has been a continual inspiration. And were it not for Professor Eugenia Kalnay de Rivas' course on numerical weather prediction and her help when I was faced with numerical problems, this thesis would clearly not have been possible.

Finally my deepest thanks to Maria Rowe, who typed this manuscript when time was running short.

TABLE OF CONTENTS

1. Introduction

One aspect of the atmosphere in mid-latitudes that has recieved insufficient attention to date is the average vertical temperature structure, shown in figure 1.1. In this graph, based on data from Oort and Rasmusson (1971), we see that the atmosphere may be divided into three regions. The lowest of these is the troposphere, extending from the ground to about 11 kilometers, where the temperature varies essentially linearly with height, the lapse rate being about 5.3 K km^{-1}. Above this lies the stratosphere, where the temperature profile is again linear, with a lapse rate of about .5 K km^{-1}. Between these two regions is the tropopause, a sharp break in the temperature profile. Considering the rather basic nature of these features, it is fairly surprising to discover that there have beem few attempts to explain their existence. Admittedly, the results of multi-layer GCMs bear a fairly close resemblance to the observations, but these models contain so many physical mechanisms that it is essentially impossible to determine which processes are relevant to the problem and which processes can be ignored. What is needed is a simple model which, because of its limited scope, clearly defines the processes contributing to the final result. It is hoped that this paper is a step in the right direction.

The simplest model of the temperature distribution in an atmosphere is the radiative equilibrium (RE) model. Given the distribution of the radiatively important gases (H_2O, CO_2, O_3) in the atmosphere, the requirement that the incoming flux of solar (visible) radiation and the outgoing flux of thermal (infrared) radiation must balance in a state of equilibrium is sufficient to determine the vertical distribution of temperature. This

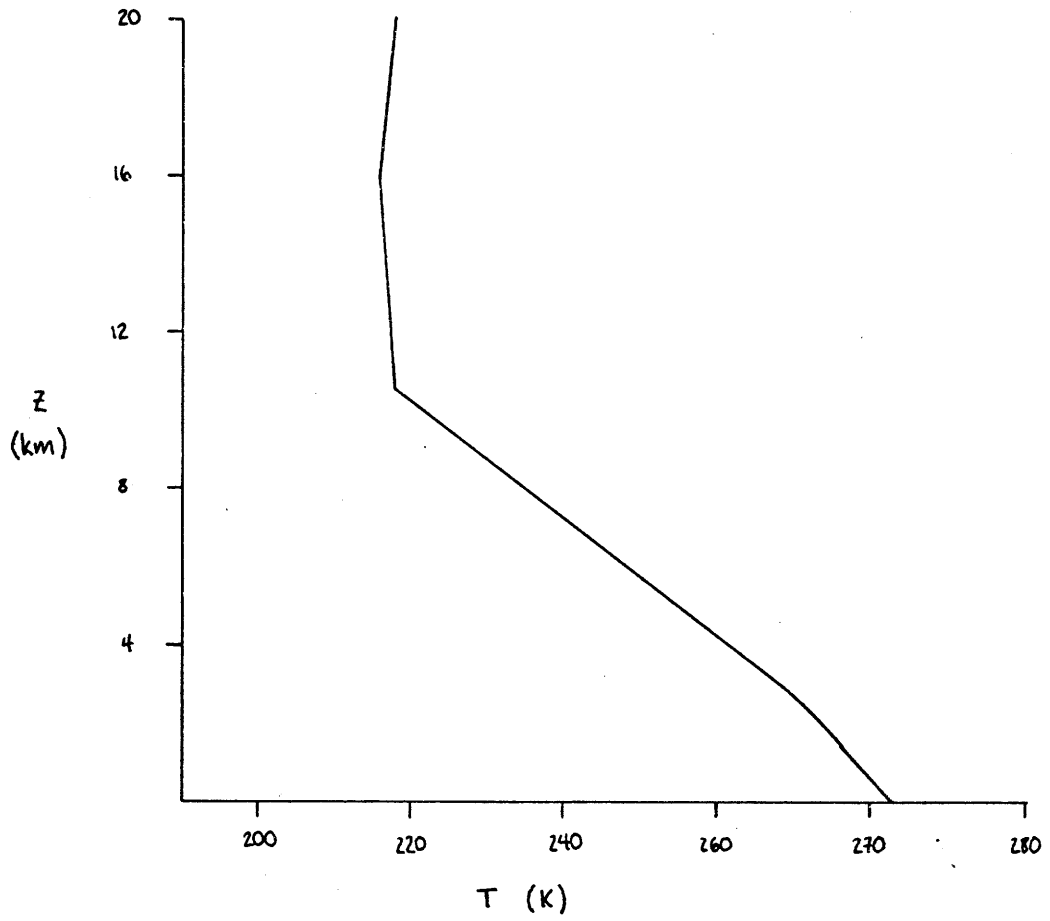

Figure 1.1 Annual average temperature as a function of height at 45° N latitude. From Oort and Rasmusson (1971)

sort of calculation has been carried out by Manabe & Weatherald (1967) for the earth's atmosphere with fixed relative humidity and surface temperature with the result shown in figure 1.2.

The RE profile shown in figure 1.2 is not, however, a very good representation of the real atmosphere-in particular the average lapse rate in the lowest 5 km is about 13 K km^{-1}, considerably greater than the dry adiabatic lapse rate of 9.8 K km^{-1}. Thus, the atmosphere is statically unstable and convection will occur until the lapse rate does not exceed 9.8 K km^{-1} anywhere in the atmosphere. Manabe and Weatherald (1967), noting that in actuality the lapse rate never exceeds 6.5 K km^{-1}, made this value the critical lapse rate at which convection occurs in a radiative-convective equilibrium(RCE) model in which radiative and convective heat fluxes are balanced; the temperature profile obtained from this model is shown in figure 1.3.

The RCE profile bears a reasonable resemblance to the observed profile of figure 1.1, and because of this the RCE model is often invoked to explain the temperature distribution in the troposphere and the existence of the tropopause. This however, is a misinterpretation of Manabe and Weatherald's results. Free thermal convection cannot occur in an atmosphere with a lapse rate of less than 9.8 K km^{-1}, so it certainly cannot contribute to the maintainance of a lapse rate of 6.5 K km^{-1}. Manabe and Weatherald realized this and pointed out that some process other than dry convection must be involved in maintaining the stable lapse rate; however, as their concern was primarily with the radiative aspects of the problem, they treated these unknown processes as convection in order to simplify the calculation.

What then is the process which maintains the statically stable profile of the mid-latitude troposphere against the destabilizing influence

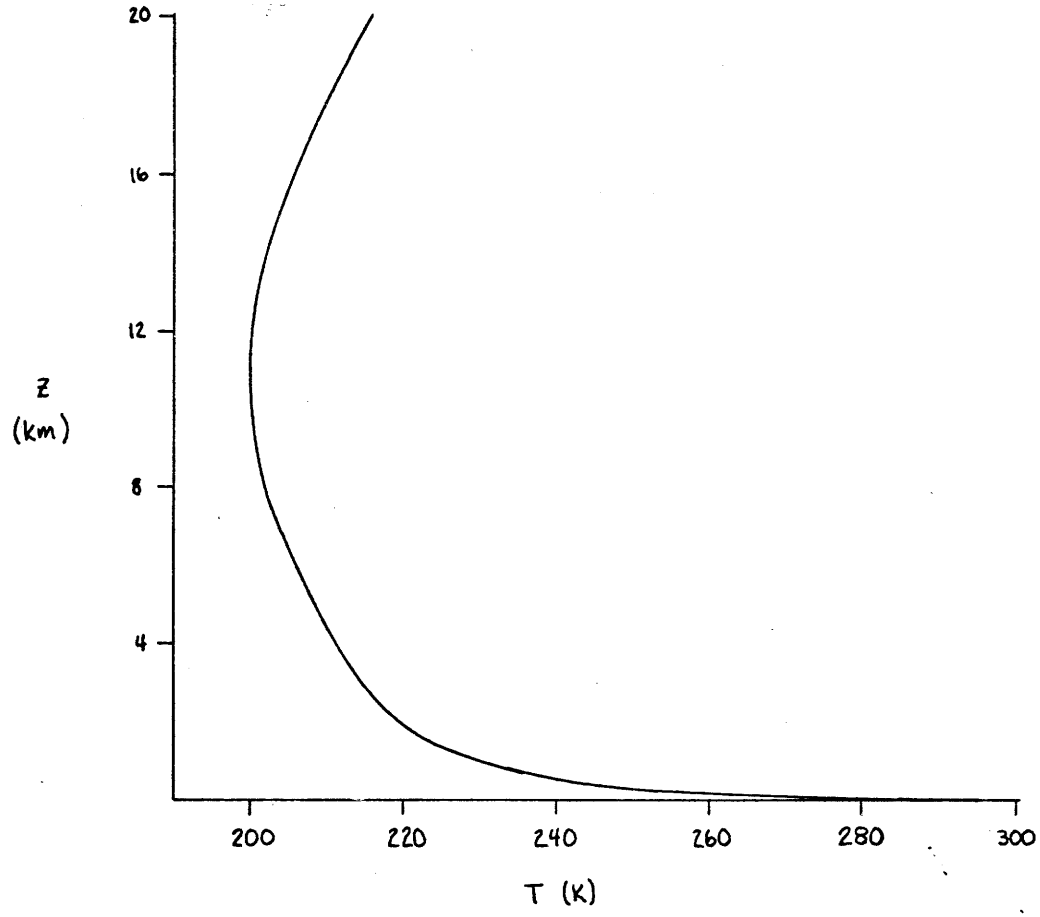

Figure 1.2 Radiative equilibrium temperature as a function of height. From Manabe and Weatherald (1969)

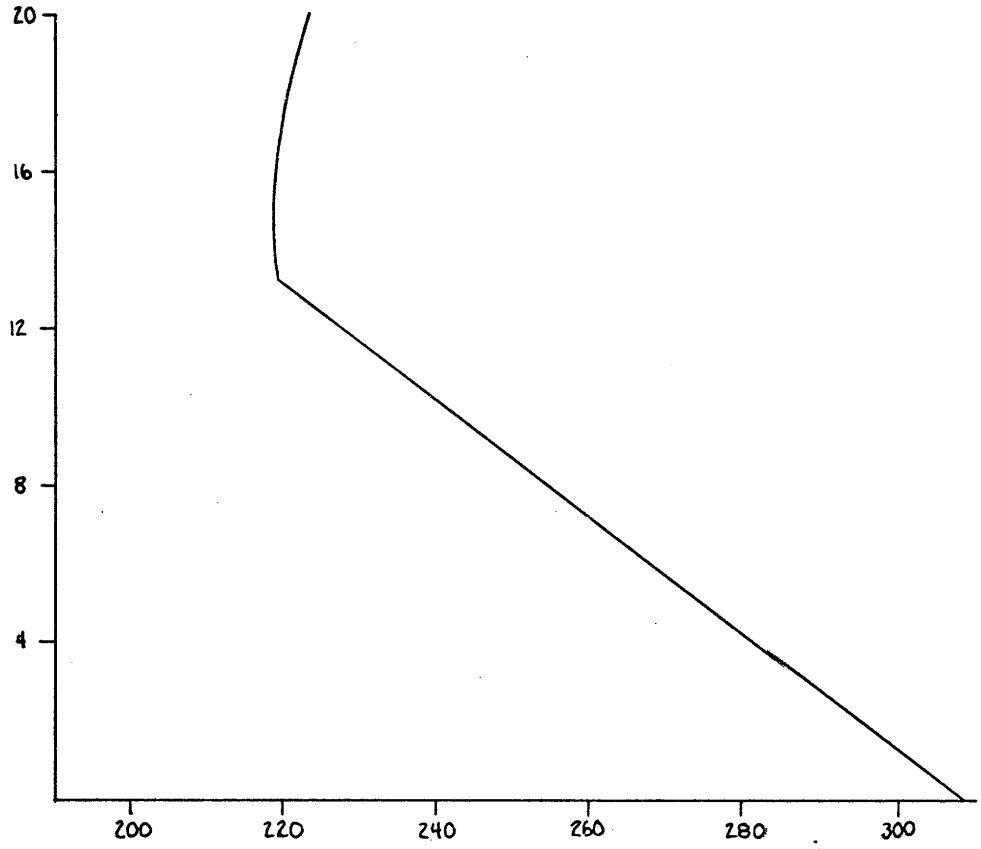

Figure 1.3 Radiative-convective equilibrium profile of Manabe and Weatherald (1969)

of radiative processes? A possible mechanism which is investigated in this paper is the upward transport of heat by large scale baroclinic eddics. Baroclinic eddies (see for example Charney, 1973) are essentially large scale convective cells which can occur in an atmosphere that is statically stable but which has a horizontal temperature gradient. To see how such convection can occur and how it can transport heat upward, we refer to figure 1.4, showing lines of constant temperature in a vertical cross section of an atmosphere which is statically stable and in which temperature decreases towards the pole. Examining this system via the "parcel" method of stability analysis, we note that an exchange of parcels along the line AB raises a denser parcel than it lowers, increasing the potential energy of the system. If, on the other hand, air parcels are exchanged along the line AC, a light parcel is raised and a heavy parcel is lowered, releasing potential energy and allowing the disturbance to grow. This sort of disturbance is baroclinic instability, a quasi-horizontal convective process which, as can be seen from the figure, transports warm air poleward and upward.

Stone (1972b) suggested that these eddies might be responsible for maintining the static stability of the atmosphere against the radiative heat fluxes and developed a simple analytical model for the radiative-dynamical equilibrium(RDE) state of the atmosphere. Using previous results from calculations of wavelength, growth rate, and heat transports of baroclinic eddies in Eady's (1949) model of baroclinic instability (Stone, 1966, 1972a), he balanced the vertical and horizontal fluxes of heat due to the eddies with the radiative fluxes and obtained a single algebraic equation for the mean tropospheric Richardson number of the RDE state. Using typical atmospheric values of the parameters in this equation, he obtained a value of 1.6 K km^{-1}

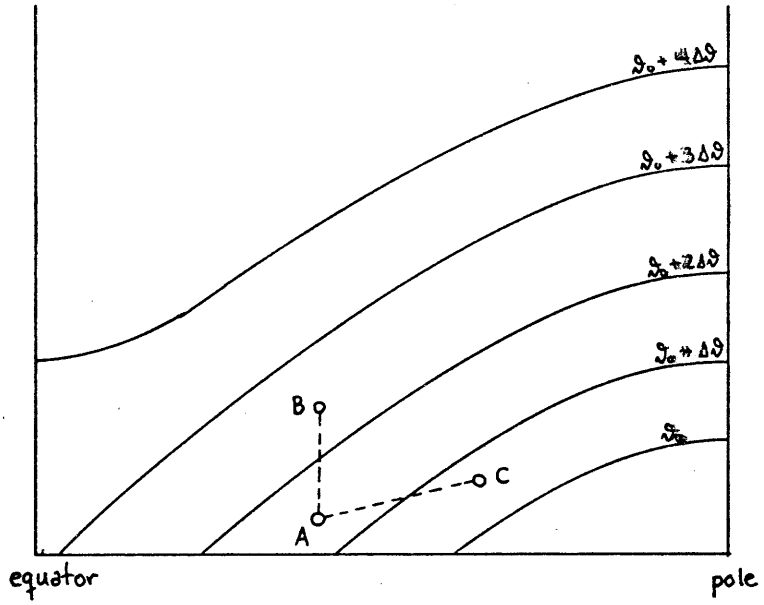

Figure 1.4 Lines of constant potential temperature in a meridional cross section of an atmosphere which is statically stable and in which the temperature decreases towards the pole. Exchange of parcels A and B increases the potential energy of the system, whereas exchange of parcels A and C decreases the potential energy and gives rise to baroclinic instability.

for the static stability (potential temperature lapse rate) of the troposphere. While this is only half the observed value of the static stability (3.3 K km^{-1}), it is a considerable improvement over the value of 0 K km^{-1} given by the dry RCE model.

Stone's model, however, only dealt with the vertically averaged static stability, not the detailed vertical temperature structure. It thus assumed that the RDE profile was linear and was incapable of dealing with such things as the tropopause. This paper is an attempt to extend Stone's model by making it one-dimensional so as to allow variations of quanitities in the vertical. The greater amount of information to be gained from such amodel naturally exacts its price: we will be forced to do a numerical calculation instead of Stone's analytic one and consequently will not be able to understand the processes at work quite as well.

2. The Model

2.1 The Predictive Equations

In this chapter we will develop the radiative-dynamical model to be used in this study. The model will make use of the Boussinesq approximation, which assumes the atmosphere to be incompressible, so that we may write the continuity equation as

$$\frac{\partial u}{\partial x} + \frac{\partial v}{\partial y} + \frac{\partial w}{\partial z} = 0 \qquad (2.1.1)$$

where u, v, and w are, resectively, the zonal, meridional, and vertical velocities. The use of this approximation in a model which includes the lowest 20 km of the atmosphere (about three density scale heights) is somewhat dubious, but as the results obtained should be qualitatively correct we will adopt the approximation to simplify the computations.

The model will be based on the thermal equation

$$\frac{\partial \vartheta}{\partial t} + u\frac{\partial \vartheta}{\partial x} + v\frac{\partial \vartheta}{\partial y} + w\frac{\partial \vartheta}{\partial z} = Q_{rad}$$

where ϑ is the potential temperature (which equals the temperature in a Boussinesq fluid) and Q_{rad} is the radiative heat flux divergence. Using the continuity equation, this may be written in flux form as

$$\frac{\partial \vartheta}{\partial t} + \frac{\partial}{\partial x}u\vartheta + \frac{\partial}{\partial y}v\vartheta + \frac{\partial}{\partial z}w\vartheta = Q_{rad}.$$

In this study, however, we are not concerned with the detailed

three-dimensional temperature structure given by this equation but in the horizontally averaged temperature structure. We thus average the above equation around a latitude circle to get

$$\frac{\partial \bar{\vartheta}}{\partial t} + \frac{\partial}{\partial y}\overline{v\vartheta} + \frac{\partial}{\partial z}\overline{w\vartheta} = \overline{Q_{rad}} \qquad (2.1.2)$$

where the overbar denotes the x average. Averaging this equation over y and requiring the meridional heat flux, $\overline{v\vartheta}$, to vanish at the as yet unspecified boundaries of the averaging region, we have

$$\frac{\partial}{\partial t}\langle\bar{\vartheta}\rangle = -\frac{\partial}{\partial z}\langle\overline{w\vartheta}\rangle + Q_{rad} \qquad (2.1.3)$$

where the angle brachets denote the y average. This is a predictive equation for the horizontally average temperature: given an initial vertical temperature profile and a knowledge of the radiative and dynamical fluxes on the right hand side of equation 2.1.3, the equation can be integrated in time to yield the vertical temperature structure at any future time. At some point the temperature will be such that the radiative and dynamical fluxes balance and we have the RDE solution which we seek.

In order to calculate the RDE state, then, we must know the fluxes on the right hand side of equation 2.1.3. As this study is primarily concerned with the effects of large scale dynamics upon the temperature structure, the radiative heating will be modelled somewhat crudely by the familiar linearized law which sets

$$Q_{rad} = \frac{1}{\tau}(\vartheta_e - \vartheta) \qquad (2.1.4)$$

where ϑ_e is the radiative equilibrium temperature and τ an appropriate radiative time constant. Putting this expression into equation 2.1.3 gives

$$\frac{\partial}{\partial t}\langle\bar{\vartheta}\rangle = -\frac{\partial}{\partial z}\langle\overline{w\vartheta}\rangle + \frac{1}{\tau}\left[\langle\bar{\vartheta}_e\rangle - \langle\bar{\vartheta}\rangle\right]. \qquad (2.1.5)$$

We will include two types of dynamical fluxes in this model: convective fluxes (to be treated in section 2.4) and fluxes due to baroclinic eddies (section 2.2). Since the driving force of the baroclinic eddies is the meridional temperature gradient (see the introduction), it is clear that a knowledge of the eddy structure at a give time requires a knowledge of the meridional temperature gradient at that time. To obtain a predictive equation for this, differentiate equation 2.1.2 with respect to y and then average over y, giving

$$\frac{\partial}{\partial t}\left\langle\frac{\partial\bar{\vartheta}}{\partial y}\right\rangle = -\left\langle\frac{\partial^2}{\partial y^2}\overline{v\vartheta}\right\rangle + \left\langle\frac{\partial\bar{Q}_{rad}}{\partial y}\right\rangle \qquad (2.1.6)$$

$$= -\left\langle\frac{\partial^2}{\partial y^2}\overline{v\vartheta}\right\rangle + \frac{1}{\tau}\left[\langle\bar{\vartheta}_e\rangle - \langle\bar{\vartheta}_y\rangle\right]$$

where it has been assumed that the vertical heat fluxes do not vary with y (this assumption will be made more explicitly in the next section).

2.2 Fluxes Due to Baroclinic Eddies

In order to calculate the fluxes due to the baroclinic eddies, we use a model somewhat similar to that used by Eady (1949) to investigate baroclinic instability. In Eady's model the basic state of the atmosphere is assumed to be a purely zonal flow (no meridional or vertical velocities) in which both the zonal velocity and potential temperature increase linearly with height. This flow is found to be unstable to small perturbations which will then grow to become finite amplitude baroclinic waves (though since the model is a linear model it is not valid for the finite amplitude waves). The model used in this study will differ from Eady's model in allowing for vertical structure in both the zonal wind and potential temperature.

The continuity, momentum, and thermal equations for a Boussinesq fluid are

$$\frac{\partial u}{\partial x} + \frac{\partial v}{\partial y} + \frac{\partial w}{\partial z} = 0$$

$$\frac{du}{dt} = fv - \frac{1}{\rho}\frac{\partial p}{\partial x}$$

$$\frac{dv}{dt} = -fu - \frac{1}{\rho}\frac{\partial p}{\partial y}$$

$$\frac{\partial p}{\partial z} = \alpha \rho g \vartheta$$

$$\frac{\partial \vartheta}{\partial t} = 0$$

where $\frac{d}{dt} = \frac{\partial}{\partial t} + u\frac{\partial}{\partial x} + v\frac{\partial}{\partial y} + w\frac{\partial}{\partial z}$ is the advective derivitive, f the Coriolis parameter, ρ the constant density, p the pressure, g the gravitational acceleration, and the thermal expansion coefficient, α is given by $\alpha = \frac{1}{T_0}$ where T_0 is the average atmospheric temperature. In writing the thermal equation in this manner, it has been assumed that the eddy time scale is small enough compared to the radiative timescale that direct radiative effects on the eddies can be neglected. We now write the fields in the above equations as

$$u = \bar{u} + u' \quad , \text{ etc.}$$

where the barred quantities are the basic state fields and the primed quantities are small perturbations on these fields. The basic state fields are given by

$$\bar{v} = \bar{\omega} = 0$$

$$\bar{\vartheta} = -m(z)y + \bar{\vartheta}(z)$$

$$\bar{u} = \bar{u}(z)$$

where $m(z) = -\frac{\partial \bar{\vartheta}}{\partial y}$ is the magnitude of the meridional temperature gradient at each level. Putting these expressions into the equations of motion and retaining only those terms which are linear in the primed quantities gives the linearized equations of motion:

$$\frac{\partial u'}{\partial x} + \frac{\partial v'}{\partial y} + \frac{\partial \omega'}{\partial z} = 0$$

$$\frac{\partial u'}{\partial t} + \bar{u}\frac{\partial u'}{\partial x} + \bar{u}_z \omega' = fv' - \frac{1}{\rho}\frac{\partial p'}{\partial x}$$

$$\frac{\partial v'}{\partial t} + \bar{u}\frac{\partial v'}{\partial x} = -fu' - \frac{1}{\rho}\frac{\partial p'}{\partial y}$$

$$\frac{\partial p'}{\partial z} = \alpha g \rho \vartheta'$$

$$\frac{\partial \vartheta'}{\partial t} + \bar{u}\frac{\partial \vartheta'}{\partial x} - m v' + \bar{\vartheta}_z \omega = 0$$

Assuming that the perturbations are baroclinic waves with no meridional structure, we write

$$u' = u(z)\, e^{i(kx + \sigma t)} = u(z)\, e^{ik(x+ct)}, \quad \text{etc.}$$

where k is the wavenumber, c the phase speed, and $\sigma = kc$ the frequency of the wave. Leaving out the meridional structure of the wave, as has been done, will create problems later, as it is the meridional variation of the horizontal heat flux which changes the meridional temperature gradient (see equation 2.1.6). Correct modelling of the meridional structure of the waves, however, requires the inclusion of the meridional variation of the basic state (see Stone, 1969) and this would complicate the present model by requiring the addition of a second dimension. We will thus ignore the meridional variation of the wave except when it is required for the evaluation of equation 2.1.6, where we will introduce a particular form for the horizontal heat flux.

Using the above form for all perturbation quantities in the linearized equations of motion, we get a system of equations in which the only variable is z :

$$iku + \frac{dw}{dz} = 0 \qquad (2.2.1)$$

$$ik(c+\bar{u})u + \bar{u}_z w = fv - \frac{ik}{\rho} p \qquad (2.2.2)$$

$$ik(c+\bar{u})v = -fu \qquad (2.2.3)$$

$$\frac{dp}{dz} = \alpha \rho g \vartheta \qquad (2.2.4)$$

$$ik(c+\bar{u})\vartheta - mv + \bar{\vartheta}_z w = 0. \qquad (2.2.5)$$

These equations may be combined to give a second order ordinary differential equation for w, the perturbation vertical velocity:

$$[f^2 - k^2(c+\bar{u})^2]w_{zz} - \frac{2f^2\bar{u}_z}{(c+\bar{u})} w_z - \alpha g k^2 \bar{\vartheta}_z w + k^2(c+\bar{u})\bar{u}_{zz} w = 0 .$$

This equation may be simplified considerably by making the quasi-geostrophic assumption, i.e. by assuming that the Rossby number of the disturbance is small compared to one. Writing the bracketed quantity in the first term as $[f^2 - k^2(c+\bar{u})^2] = f^2\left[1 - \frac{k^2(c+\bar{u})^2}{f^2}\right]$ we recognize the second term of this sum as the square of the Rossby number and thus neglect it. Then comparing the last term in the equation to what remains of the first, we have $\frac{k^2(c+\bar{u})^2\bar{u}_{zz} w}{f^2 w_{zz}} \sim \frac{k^2\bar{u}^2}{f^2}$, again the

square of the Rossby number. Thus, with the quasi-geostrophic asssumption, the equation for the perturbation vertical velocity is

$$f^2 w_{zz} - \frac{2f^2 \bar{u}_z}{(c+\bar{u})} w_z - \alpha g k^2 \bar{\theta}_z w = 0 \qquad (2.2.6)$$

Equation 2.2.6 is of the form

$$D(z; c, k)\, w = 0$$

where D is a second order non-linear (the coefficients depend on z through $\bar{u}$ and $\bar{\theta}$) differential operator which has a parametric dependence on c and k . This equation, with two boundary conditions on w , constitutes an eigenvalue problem for c and k ; given a value of k there are only certain values of c for which both the equation and the boundary conditions on w are satisfied. One of these is easy enough to come by: we simply require that w vanish at the earth's surface ($z = 0$). The other boundary condition should presumably be some sort of radiation condition at $z = \infty$ but this would be difficult to use in our model, so we will instead require that w also vanish at some height, $z = h$, in the atmosphere. If we pick h to lie in the stratosphere, the high static stability there should lead to small w anyway, so setting w equal to zero should not drastically affect the results.

The details of the solution of the eigenvalue problem presented by equation 2.2.6 are given in Appendix A. Essentially, the derivatives in equation 2.2.6 are replaced by finite difference representations based on

the values of w and ϑ at N specified levels $z_1, z_2, \ldots z_N$ (see figure 2.2.1), resulting in a system of N algebraic equations for $\omega_1, \omega_2, \omega_3, \ldots \omega_N$. The eigenvalues of this system of equations are the roots of a polynomial of order N in $(c+\bar{u})$; had the approximations leading to equation 2.2.6 not been made, the polynomial would have been of order 3N requireing more computer time and creating problems with computational stability. When the resulting problem is solved, one gets, for a specific value of k, N possible values of c; these values are the phase speeds for $\frac{N}{2}$ pairs of growing and damped baroclinic modes. For this problem we pick the gravest baroclinic mode, as this has the fastest growth rate and is thus likely to dominate the flow at finite amplitude.

To find the structure of the gravest baroclinic mode, one solves the eigenvalue problem for a particular value of k and then puts this k and its associated c back into the system of algebraic equations for $\omega_1, \omega_2, \ldots \omega_N$, (equation A.6) and solves for the value of ω at the N levels. To compute the other relevant fields, we note that from equations 2.2.1, 2.2.3, and 2.2.5

$$u = \frac{i}{k} \frac{d\omega}{dz} \tag{2.2.7}$$

$$v = \frac{i}{k(c+\bar{u})} f u \tag{2.2.8}$$

$$\theta = \frac{i}{k(c+\bar{u})} [\delta_z \omega - m v] . \tag{2.2.9}$$

Written in finite difference form, these allow one to compute the temperature and meridional velocity fields of the eddy from a knowledge of

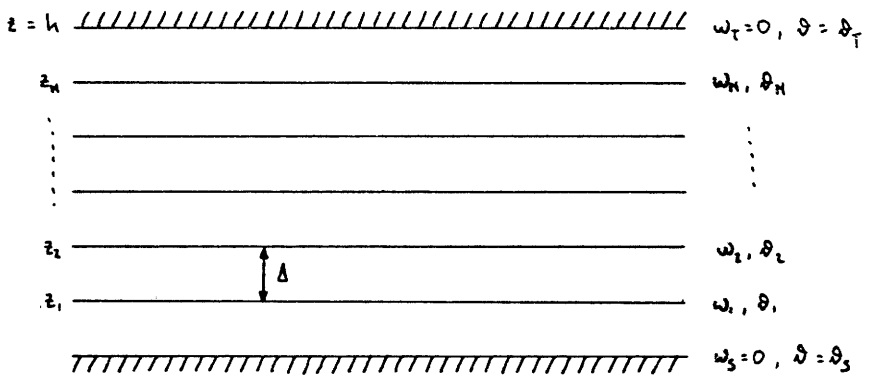

Figure 2.2.1 The vertical grid used in solving the eigenvalue problem for the eddies

$\omega_1, \omega_2, \ldots \omega_N$.

In the preceeding analysis of the baroclinic eddies, the assumption was made that the amplitude of the eddies was small enough that the equations of motion could be linearized about the basic state. The result of this assumption is that the solution for the eddies has an unknown amplitude which grows exponentially with time. In a physical flow the eddies would soon reach a large enough amplitude that they would interact with the mean flow, changing the flow and eventually reaching some sort of equilibrium with it. As a linear model like ours is not capable of describing this equilibration process, it will thus be necessary to add it as a seperate part of the model.

A detailed approach to the finite amplitude problem is quite complex (see e.g., Pedlosky,1970) and well beyond the scope of this model, so we will have to use a much simpler approach. The two bits of knowledge required are the structure and the amplitude of the eddy when it has equilibrated with the mean flow. The first is easily dealt with by making the so-called "shape assumption", i.e. by assuming that the structure of the finite amplitude wave is the same as that of the linear wave. Thus we assume that the ω, v, and ϑ fields of the finite amplitude wave are given by equations 2.2.6, 2.2.8, and 2.2.9 but that these fields are multiplied by some complex amplitude factor A.

To determine the amplitude factor, we note that in Pedlosky's (1970) model, an inviscid flow with $\beta = 0$ (section 6 of Pedlosky) equilibrates when the perturbation meridional velocity is of the same order as the total shear of the zonal flow (if the meridional and zonal wavelengths of the disturbance are approximately equal). This appears to be true of flows in the laboratory and nature as well, and since the total shear of the zonal

flow is of the same order as the zonal velocity, we will pick the amplitude so that the eddy meridional velocity, $A v$, is of the order of $\bar{u}$. Thus we write

$$\int_0^h |A|^2 v^* v \, dz = \int_0^h \bar{u}^2 \, dz$$

or

$$|A|^2 = \int_0^h \bar{u}^2 \, dz \Big/ \int_0^h v^* v \, dz$$

where the asterisk denotes the complex conjugate. This result is by no means exact, though, so the model should be checked for its sensitivity to the amplitude.

Given the amplitude of the wave, we are now in a position to compute the heat fluxes $\overline{v\vartheta}$ and $\langle\overline{w\vartheta}\rangle$ required by equations 2.1.5 and 2.1.6 It should be noted that in the notation of the present section these fluxes are $\overline{\mathrm{Re}[v e^{i(kx+\sigma t)}] \cdot \mathrm{Re}[\vartheta e^{i(kx+\sigma t)}]}$ and $\overline{\mathrm{Re}[w e^{i(kx+\sigma t)}] \cdot \mathrm{Re}[\vartheta e^{i(kx+\sigma t)}]}$ respectively. To simplify these expressions, we ignore the time dependence (which does not enter any of the calculations), do a bit of algebra, and perform the x average, getting

$$\begin{aligned}
\overline{v\vartheta} &= \overline{\mathrm{Re}[v e^{ikx}] \, \mathrm{Re}[\vartheta e^{ikx}]} \\
&= \overline{\mathrm{Re}[(v_r + i v_i)(\cos kx + i \sin kx)] \, \mathrm{Re}[(\vartheta_r + i\vartheta_i)(\cos kx + i \sin kx)]} \\
&= \tfrac{1}{2}(v_r \vartheta_r + v_i \vartheta_i) \\
&= \tfrac{1}{2} \mathrm{Re}(v \vartheta^*) \, .
\end{aligned}$$

Similarly,

$$\langle \overline{\omega\vartheta} \rangle = \tfrac{1}{2} \mathrm{Re}\,(\omega\vartheta^*).$$

As noted before, the present form of the meridional flux is not adequate for the model because it lacks the y dependence which will contribute to the change in the meridional gradient through the flux divergence in equation 2.1.6. We will thus add a meridional variation to the flux by multiplying $\frac{1}{2}\mathrm{Re}\,(v\vartheta^*)$ by $6\frac{y}{L}(1-\frac{y}{L})$, where L is the distance over which the flux goes from zero through a maximum and back to zero. That this is a fairly good representation of the flux may be seen from figure 2.2.2, which shows the meridional heat flux due to transient eddies as determined by Oort and Rasmusson (1971) plotted with a parabola which goes to zero at $20^\circ N$ latitude and the pole ($L \sim 8000$ km). That this form agrees well with the data arises from the fact that in an expansion of the flux in, say, Legendre polynomials, the lowest order term, representing a heat flux across the equator, must vanish identically so that the first term in the expansion resembles a parabola. Thus we write

$$\overline{v\vartheta} = 3\frac{y}{L}(1-\frac{y}{L})\,\mathrm{Re}\,v\vartheta^* .$$

Putting the expressions for $\overline{v\vartheta}$ and $\langle\overline{\omega\vartheta}\rangle$ into equations 2.1.5 and 2.1.6 gives

$$\frac{\partial}{\partial t}\langle\bar{\vartheta}\rangle = -\tfrac{1}{2}|A|^2\frac{d}{dz}\mathrm{Re}\,\omega\vartheta^* + \tfrac{1}{\tau}[\langle\bar{\vartheta}_e\rangle - \langle\bar{\vartheta}\rangle] \qquad (2.2.11)$$

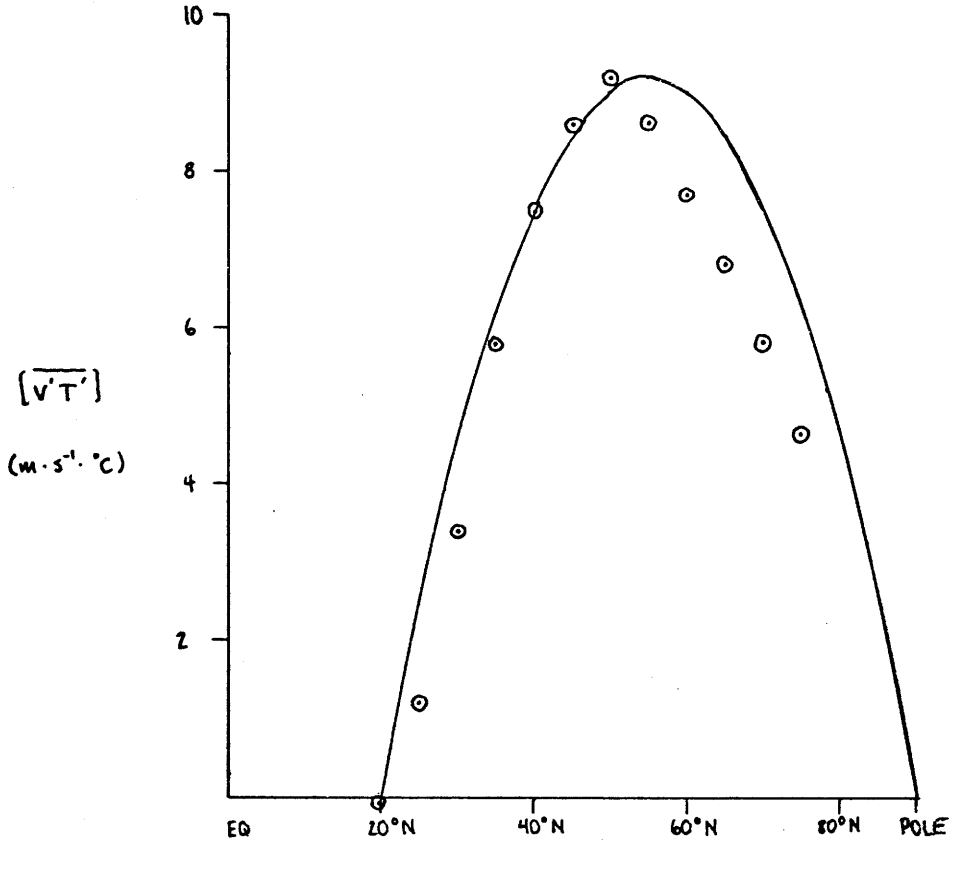

Figure 2.2.2 Yearly average mean sensible heat transport due to transient eddies, $[\overline{v'T'}]$ as a function of latitude. From Oort and Rasmusson (1971)

⊙ Oort and Rasmusson's data

—— parabolic fit to data

and

$$\frac{\partial}{\partial t}\langle\bar{\vartheta}_y\rangle = \frac{6}{L^2}|A|^2 Re\, v\vartheta^* + \frac{1}{\tau}\left[\langle\bar{\vartheta}_{e_y}\rangle - \langle\bar{\vartheta}\rangle\right] \qquad (2.2.12)$$

These are the predictive equations to be used in our model; equation 2.2.11 is applied at each of the levels in the model while equation 2.2.12 is applied only in a vertically averaged sense.

The reason for the restriction on the use of equation 2.2.12 is that a one dimensional model cannot incorporate processes (such as horizontal variations of the vertical heat flux) which play an important role in determining the meridional temperature gradient. Thus, what we will do is specify the shape of the vertical distribution of $\langle\bar{\vartheta}_y\rangle$ and use equation 2.2.12 to determine its magnitude. Figure 2.2.3 shows the vertical distribution of the mean zonal wind speed at $45^\circ N$ as determined by Oort and Rasmusson (1971). We will use this to specify the shape of the $\bar{u}$ profile and thus, through the thermal wind relation, the $\langle\bar{\vartheta}_y\rangle$ profile used in the model. The nearly linear $\bar{u}$ profile below 11 km in figure 2.2.3 indicates that the meridional temperature gradient is a constant, say ϑ_y^{obs}, in this region. If we average equation 2.2.12 over the region, we have an equation telling how this averaged gradient, ϑ_y^{mod}, changes with time in the model. Then at any time we will determine the $\bar{u}$ and $\langle\bar{\vartheta}_y\rangle$ profiles needed by the model from the observed profiles $\bar{u}_{obs}$ and $\langle\bar{\vartheta}_y\rangle_{obs}$ by the relations

$$\bar{u} = \frac{\vartheta_y^{mod}}{\vartheta_y^{obs}}\,\bar{u}_{obs}$$

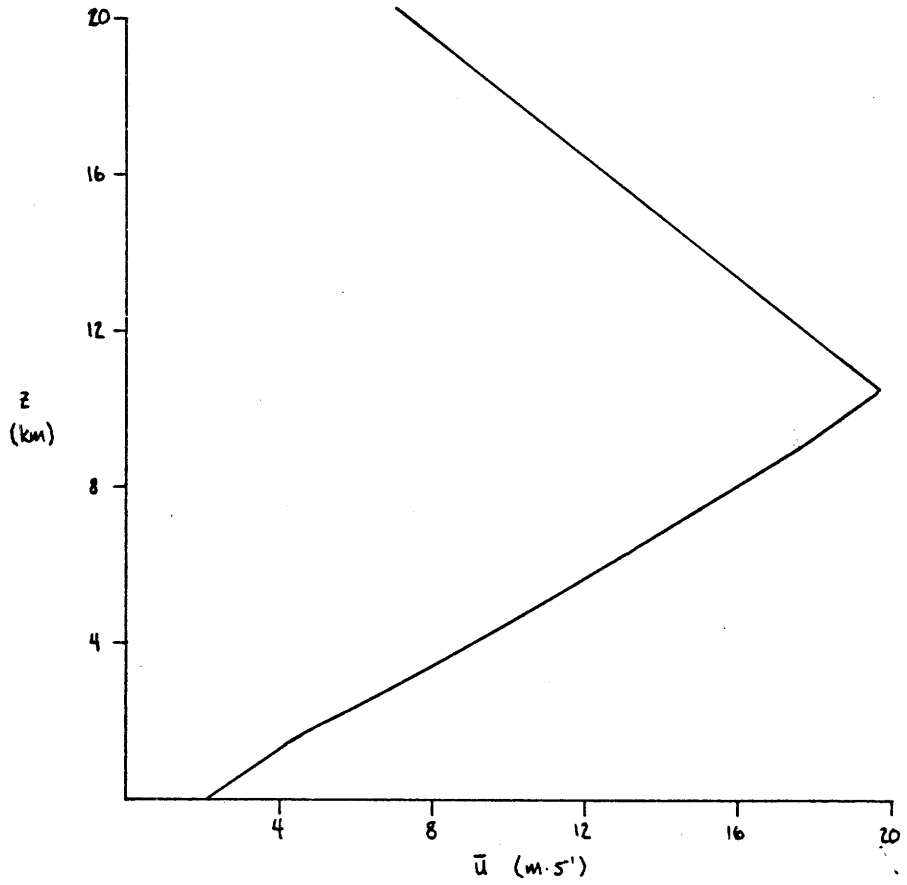

Figure 2.2.3 Annual average mean zonal wind at 45° N latitude as a function of height. From Oort and Rasmusson (1971)

and

$$\langle \bar{s}_y \rangle = \frac{\vartheta_y^{mod}}{\vartheta_y^{obs}} \langle \bar{s}_y \rangle_{obs} .$$

The profiles thus always have the same shape as the observed profiles but their amplitude is greater or less than observed depending on whether ϑ_y^{mod} is greater or less than ϑ_y^{obs} .

2.3 Integration of the Predictive Equations

In order to find the RDE state it should thus only be necessary to integrate equations 2.2.11 and 2.2.12 forward in time from some initial state until an equilibrium profile is reached. It should be pointed out here that while the process to be described below will be refered to as a "time integration", it is really an iterative procedure based on the notion of a time integration. Thus the initial profile will actually be an initial guess of the RDE temperature structure and equations 2.2.11 and 2.2.12 will be used to make corrections to this profile in a manner similar to finding the zeros of a function by Newton's method. This distinction is made because the major concern is with the equilibrium state, not with the details of how the state is reached. Thus it may on occasion be convenient to use a numerical procedure which, while not strictly valid for a time integration, will be good when applied to an equilibrium state. With this explanatory note,we return to the language of time integration.

The integration of equation 2.2.12 is fairly straightforward; given the temperature structure at a particular timestep, we use the model of baroclinic instability to compute the eddy flux divergence on the right hand side of the equation and then do a forward timestep. Thus, with $\langle \bar{\vartheta}_y \rangle^n$ denoting $\langle \bar{\vartheta}_y \rangle$ at the n^{th} timestep, equation 2.2.12 is written as

$$\frac{1}{\Delta t}\left[\langle \bar{\vartheta}_y \rangle^{n+1} - \langle \bar{\vartheta}_y \rangle^n\right] = \frac{6}{L^2}|A|^2 \, Re\, v^n \vartheta^{n*} + \frac{1}{\tau}\left[\langle \bar{\vartheta}_{e_y} \rangle - \langle \bar{\vartheta}_y \rangle^n\right]$$

so that the new meridional temperature gradient is

$$\langle \bar{\vartheta}_y \rangle^{n+1} = \langle \bar{\vartheta}_y \rangle^{n} + \Delta t \left\{ \frac{6}{L^2} |A|^2 \, \mathrm{Re}\, v^n \vartheta^{n*} + \frac{1}{\tau} \left[\langle \bar{\vartheta}_{e_y} \rangle - \langle \bar{\vartheta}_y \rangle^n \right] \right\} \qquad (2.3.1)$$

where Δt is the length of the timestep.

More care must be used in the integration of equation 2.2.11. After many months of encountering a numerical instability that did not succumb to the use of a smaller timestep interval, Δt, the author finally discovered that the equation is a disguised diffusion equation with a non-constant diffusion coefficient and is thus unstable when a forward or leap-frog timestep is used. To see this, recall that by equation 2.2.9

$$\vartheta = \frac{i}{k(c+\bar{u})} \left(\langle \bar{\vartheta} \rangle_z \omega - mv \right)$$

so that the eddy flux on the right hand side of equation 2.2.11 is

$$\frac{1}{2} |A|^2 \, \mathrm{Re}\, \omega^* \vartheta = \frac{|A|^2}{2} \mathrm{Re} \left[\frac{i}{k(c+\bar{u})} \left(\langle \bar{\vartheta} \rangle_z |\omega|^2 - m \omega^* v \right) \right]$$

$$= \frac{|A|^2 |\omega|^2 c_i}{2k^2 |c+\bar{u}|^2} \langle \bar{\vartheta}_z \rangle - \frac{m|A|^2}{2k} \mathrm{Re} \left(\frac{i \omega^* v}{c+\bar{u}} \right)$$

$$= \mu \langle \bar{\vartheta} \rangle_z - F$$

where

$$\mu = \frac{c_i |A|^2}{2} \frac{|\omega|^2}{k |c+\bar{u}|^2}$$

and

$$F = \frac{m|A|^2}{2k} \, Re\left(\frac{i\omega^4 \nu}{c+\bar{u}}\right) .$$

Thus, equation 2.2.11 may be written as

$$\frac{\partial}{\partial t}\langle\bar{\vartheta}\rangle = -\frac{\partial}{\partial z}\mu\frac{\partial}{\partial z}\langle\bar{\vartheta}\rangle + \frac{\partial F}{\partial z} + \frac{1}{\tau}\left[\langle\bar{\vartheta}_e\rangle - \langle\bar{\vartheta}\rangle\right] \qquad (2.3.2)$$

where the diffusion term is explicitly exhibited as the first term on the right hand side.

The time differencing scheme used to avoid the numerical instability arising from this term was the Crank-Nicholson scheme, an implicit scheme which is discussed in Appendix B. One characteristic of this scheme is that it requires values of the temperature at the upper and lower boundaries to obtain a solution to equation 2.3.2; it should be emphasized that these are <u>not</u> required by the physics of the problem, but are only needed by this particular computational scheme. These boundary conditions and processes other than the baroclinic eddy transports are the subject of the next section.

2.4 Boundary Layer Heat Flux, Surface Temperature, and Convective Adjustment

The preceding discussion has been limited to processes occuring in the free atmosphere. In reality there is a lower boundary to the atmosphere and heat fluxes across this boundary will be important in determining the atmosphere's thermal structure. Rather than including a detailed model of the boundary layer in our computations, however, we will simply specify the sensible heat flux from the surface to the atmosphere. Over ground, this flux is of the order of 100 to 200 $W\ m^{-2}$ (Taylor, 1956; Yap, Black, & Oke, 1974) and over the ocean it is about 20 $W\ m^{-2}$(Pond, et.al., 1971) . Averaging these values and accounting for the fact that there will be a small flux from the atmosphere to the ground at night, we will pick a value of

$$H = 50\ W\ m^{-2} \qquad (2.4.1)$$

for the boundary layer heat flux.

We will assume that this heat flux is deposited in the lowest layer of the atmosphere, so that the total amount of heat, ΔH , added to this layer in the period of time Δt (one timestep) is $\Delta H = H\Delta t$. The columnar mass of the lowest layer is $\rho\Delta$ where ρ is the density and Δ the layer thickness, so the columnar heat capacity is $c_p\rho\Delta$ and the change in temperature of the lowest layer at each timestep due to the heat flux is

$$\Delta\vartheta_1 = \frac{\Delta H}{c_p \rho \Delta} = \frac{H \Delta t}{c_p \rho \Delta} \quad . \qquad (2.4.2)$$

For the lower temperature boundary condition required by the Crank-Nicholson scheme, we will simply extrapolate downward from the temperatures at the two lowest levels in the free atmosphere in the previous timestep. Since in most cases these two levels will lie within a convecting region (i.e. a region of neutral stability) this will usually mean setting the surface temperature equal to the temperature at the lowest level. In actuality there will always be an unstable region close to the surface which gives rise to the surface sensible heat flux, but this region is restricted enough in vertical extent that it will not affect the eddy dynamics. The use of temperatures from the previous timestep to obtain the surface temperature is one of the numerical procedures mentioned previously which, while not accurate in a time-marching problem, is legitimate for an equilibrium state.

Because of the high static stability of the stratosphere, dynamical effects at the upper boundary will be small. We will thus set the temperature there equal to the radiative equilibrium temperature.

If for some reason (such as the boundary layer heat fluxes) a portion of the atmosphere becomes statically unstable, a convective adjustment is needed to bring it back to neutral stability. Consider the two levels, shown in figure 2.4.1 at which we know the temperature. Each of these levels is considered to be at the center of a layer of air of thickness Δ, and the temperature at a level is taken to be the average temperature of the corresponding layer. If the temperature of the lower layer, ϑ_n, is less than that of the upper layer,

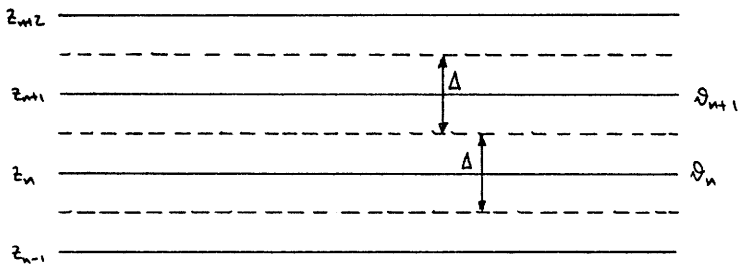

Figure 2.4.1 The layers of the atmosphere, centered on the grid levels, which are used to do convective adjustments

ϑ_{n+1} , the configuration is stable and nothing need be done. If, however, $\vartheta_{n+1} < \vartheta_n$, the system is unstable and convection will occur, mixing the air masses adiabatically until both layers are at the same temperature ϑ' . If the total heat is to remain constant (i.e. if the process is to be adiabatic), the temperature of the layers after convection must be

$$\vartheta' = \tfrac{1}{2}(\vartheta_n + \vartheta_{n+1}) . \qquad (2.4.3)$$

To adjust an unstable temperature profile, we start at the bottom of the atmosphere and compare two adjacent layers. If the layers are stable, we move up one level and compare the next two layers. If the configuration is unstable, we perform the adjustment given by equation 2.4.3 and then move up to check the next two layers. When we reach the top of the atmosphere we return to the bottom and start again, continuing until there are no regions of instability left.

2.5 Computation of the Equilibrium Profile

Having developed the details of the model, we now proceed to the calculation of the RDE equilibrium state. Given k and a temperature profile, the eigenvalue problem (equation 2.2.6) is solved for ω, which is then used to compute u, v, and ϑ from equations 2.2.7, 2.2.8, and 2.2.9, and from these the amplitude of the wave is calculated (equation 2.2.10). A forward timestep is then made using equations 2.3.1 and 2.3.2, the heat from the boundary layer is added to the lowest atmospheric layer (equation 2.4.2), and a convective adjustment is performed if necessary (equation 2.4.3). This procedure, shown in the flow diagram of figure 2.5.1, is continued until an equilibrium profile is reached.

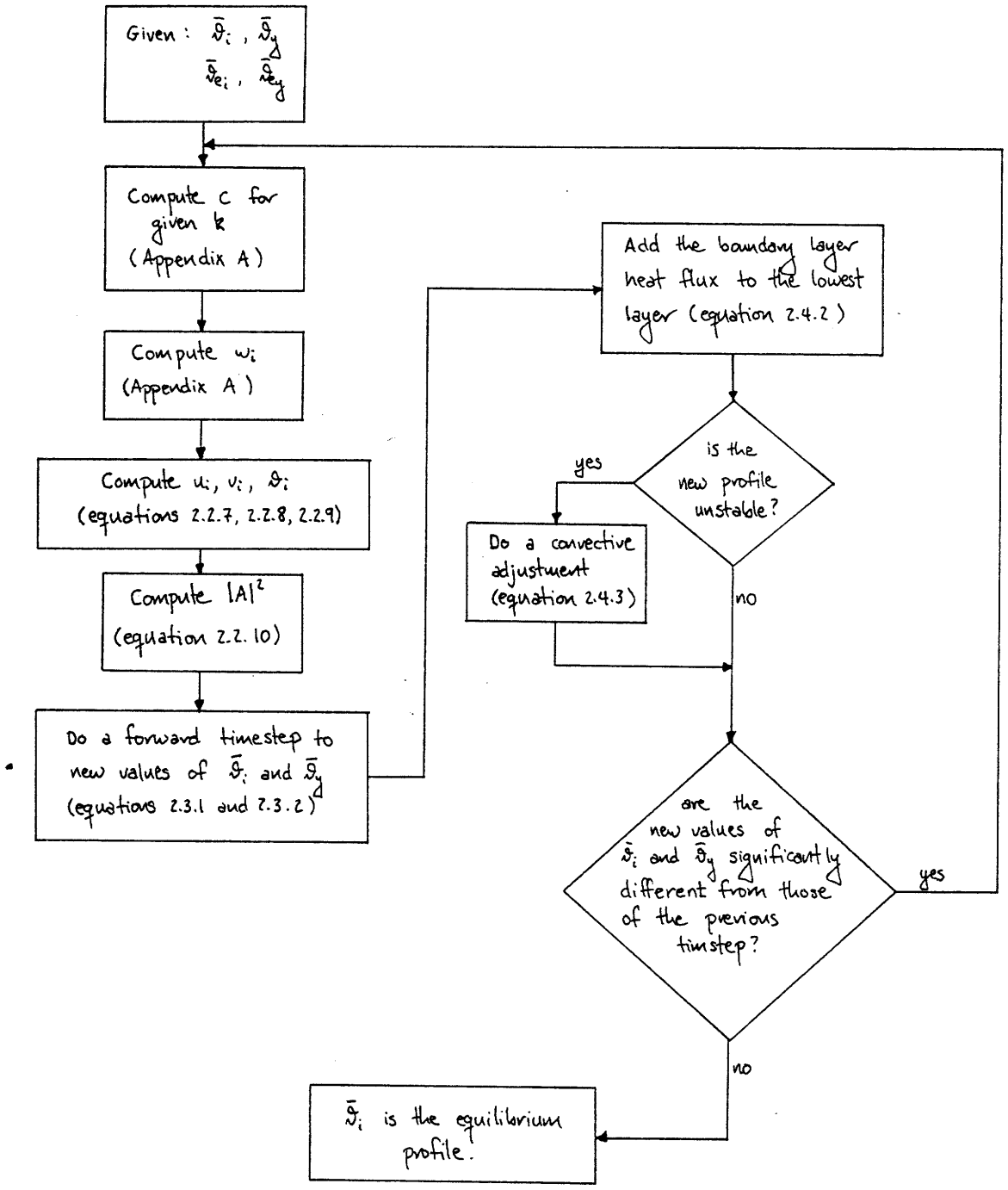

Figure 2.5.1 Flow chart for the radiative-dynamical equilibrium calculation.

3. Results

3.1 Radiative Convective Equilibrium

Before proceeding with the full radiative-dynamical equilibrium calculation we will compute the radiative-convective profile which we get by leaving the eddy dynamics out of the model. This will serve several purposes. First, by repeating Manabe and Weatherald's radiative-convective calculation we will be able to check the present model and, in particular, see how well the Newtonian cooling law of equation 2.1.4 approximates their more detailed radiative calculation. Also, comparison of a true RCE calculation (one in which convection gives a neutral lapse rate rather than the stable rate used by Manabe and Weatherald) with the full radiative-dynamical calculation will enable us to distinguish between the effects of radiation and convection and the effects of the baroclinic eddies.

In all the model runs to be discussed in this chapter the upper boundary at which we set ω to zero is taken to be at 21 kilometers, and between this height and the ground there are, at one kilometer intervals, 20 levels at which the various fields will be computed. We must also specify a number of quantities at these levels. The potential temperature of the radiative equilibrium state, ϑ_e , will be that computed from the radiative model of Manabe and Weatherald. This ϑ_e profile is shown in figure 3.1.1. The profile of the zonal wind, $\bar{u}$, will be that of figure 2.2.3, and from this the profiles of $\bar{u}_z$ and $\bar{\vartheta}_y$ will be calculated. The meridional gradient of the radiative equilibrium temperature, $\bar{\vartheta}_{e_y}$, at 45° N can be computed from satellite observations of

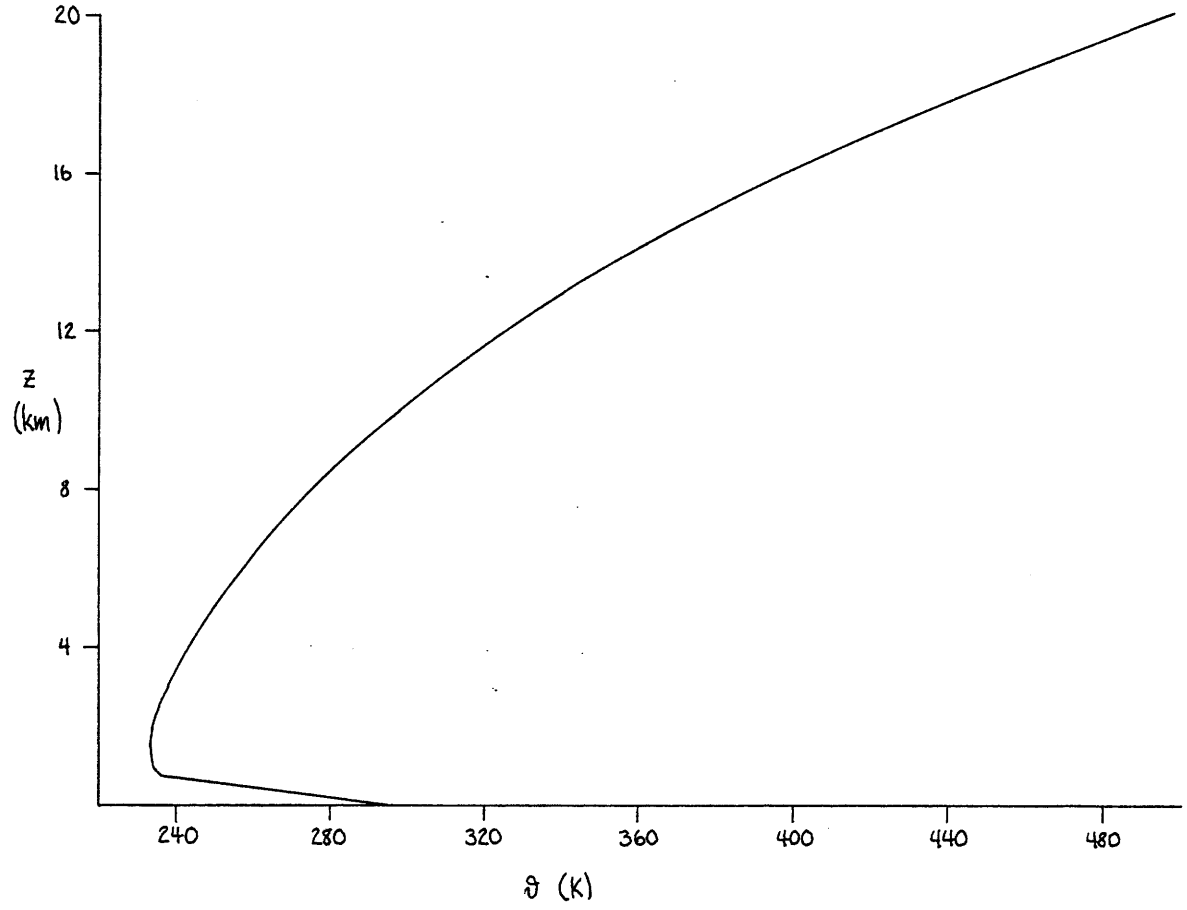

Figure 3.1.1 Potential temperature as a function of height for the radiative equilibrium model of Manabe and Weatherald (1969)

albedo, and is found to be about 1.3×10 K km^{-1}. The time step used in the calculations was $\Delta t = 0.2$ day, relatively short compared to the typical time scale of a few days for baroclinic waves.

For the radiative time constant of the troposphere we will pick the constant value $\tau = 30$ days. In actuality the radiative properties of the atmosphere, and thus the time constant, vary with height, but this refinement will not be included in our model. To see how the results depend on the value of τ that we choose, calculations will also be done for $\tau = 20$ days and $\tau = 40$ days. These calculations will also serve another purpose, as can be seen by writing equation 2.2.11, the predictive equation for the vertical temperature structure, in its equilibrium form (i.e. for $\frac{\partial}{\partial t} = 0$):

$$|A|^2 \tau \frac{d}{dz} \mathrm{Re}\, \omega^* \vartheta = 2[\langle \bar{\vartheta}_e \rangle - \langle \bar{\vartheta} \rangle].$$

Inspecting this equation, we see that τ only enters the problem through the product $|A|^2\tau$, $|A|^2$ being the amplitude of the baroclinic wave. Thus it is the relative magnitudes of the radiative time constant and the eddy amplitude which determine the temperature structure, not their separate absolute magnitudes: a system with vigorous eddies and large radiative fluxes (large $|A|^2$, small τ) can have the same vertical temperature struture as one with weak eddies and small radiative fluxes (small $|A|^2$, large τ) provided the product $|A|^2\tau$ is the same for both systems. A calculation in which we keep $|A|^2$ constant and change τ by a factor of a may thus be interpreted as one in which τ is held constant and $|A|$ is changed by the factor $a^{1/2}$.

To compare our model to the RCE model of Manabe and Weatherald, we

note that in their equilibrium profile (figure 3.1.2) the potential temperature lapse rate in the lower half of the atmosphere is 4.9 $K\,km^{-1}$. We will thus leave the baroclinic eddies out of the model and take the critical lapse rate at which convection occurs to be 0 $K\,km^{-1}$. The result of this calculation for $\tau = 30$ days and $H = 50\ W\ m^{-2}$ (equation 2.4.1) is shown in figure 3.1.3. We see from this figure that our model has a much shallower convective region than that of Manabe and Weatherald (8 kilometers in our model as opposed to 13.5 kilometers in theirs) and that the atmosphere in our model is also considerable colder than theirs. The reason for this difference is not entirely clear, though it is probably due to a difference in the heat flux from the lower boundary. To see how this heat flux affects the profile in our model, figure 3.1.4 shows the result of calculations for heat fluxes of $H = 25$, $H = 50$, and $H = 100$ $W\ m^{-2}$; we see that increasing the flux raises the temperature of the lower atmosphere and increases the depth of the convecting layer. It appears that a boundary layer heat flux of 400-500 $W\ m^{-2}$ would be sufficient to bring our profile into correspondence with that of Manabe and Weatherald. Heat fluxes of this magnitude could be obtained by the inclusion of latent heat fluxes as well as the sensible heat flux which we have specified, but the inclusion of latent heat would require some sort of mechanism for its release via condensation, which would make the model considerably more complicated. Furthermore, without knowing the value of the boundary layer flux obtained in Manabe and Weatherald's computation we cannot be sure that this flux, rather than some other difference, is the cause of the discrepancy between the models. Thus we will stick with the value of $H = 50\ W\ m^{-2}$ as the "best value" of the surface heating and interpret

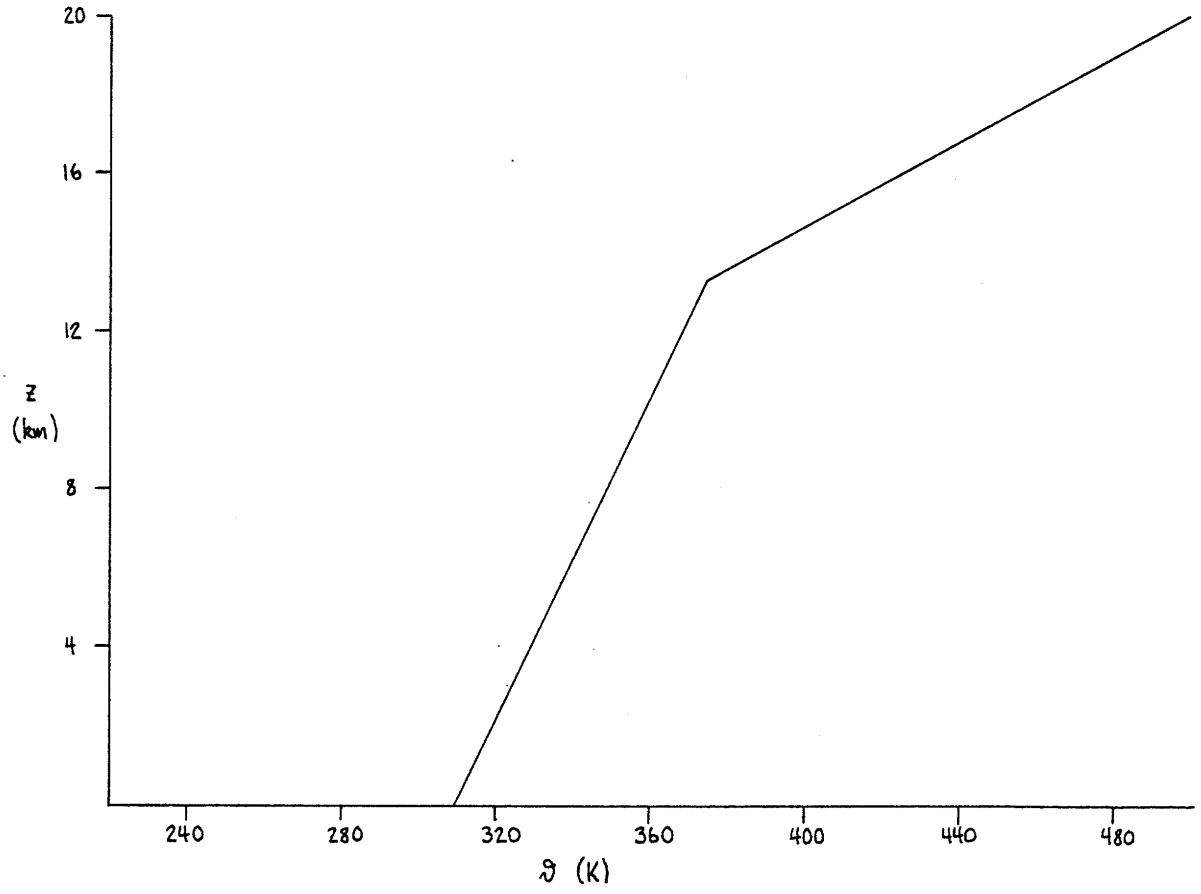

Figure 3.1.2 Potential temperature as a function of height for the radiative-convective equilibrium model of Manabe and Weatherald.

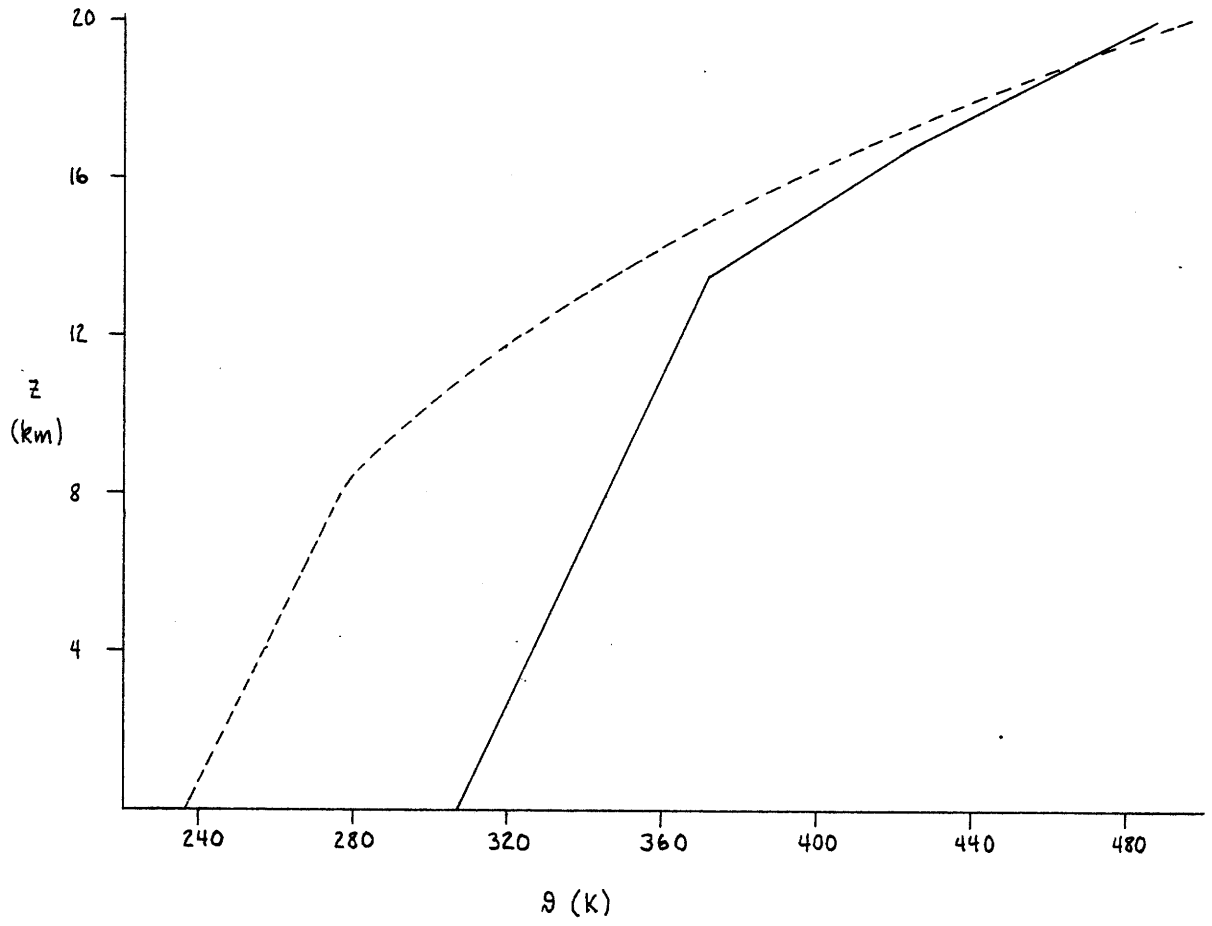

Figure 3.1.3 The radiative - convective equilibrium solution of Manabe and Weatherald (solid line) and the RCE solution computed with the present model using the critical lapse rate of Manabe and Weatherald (dashed line).

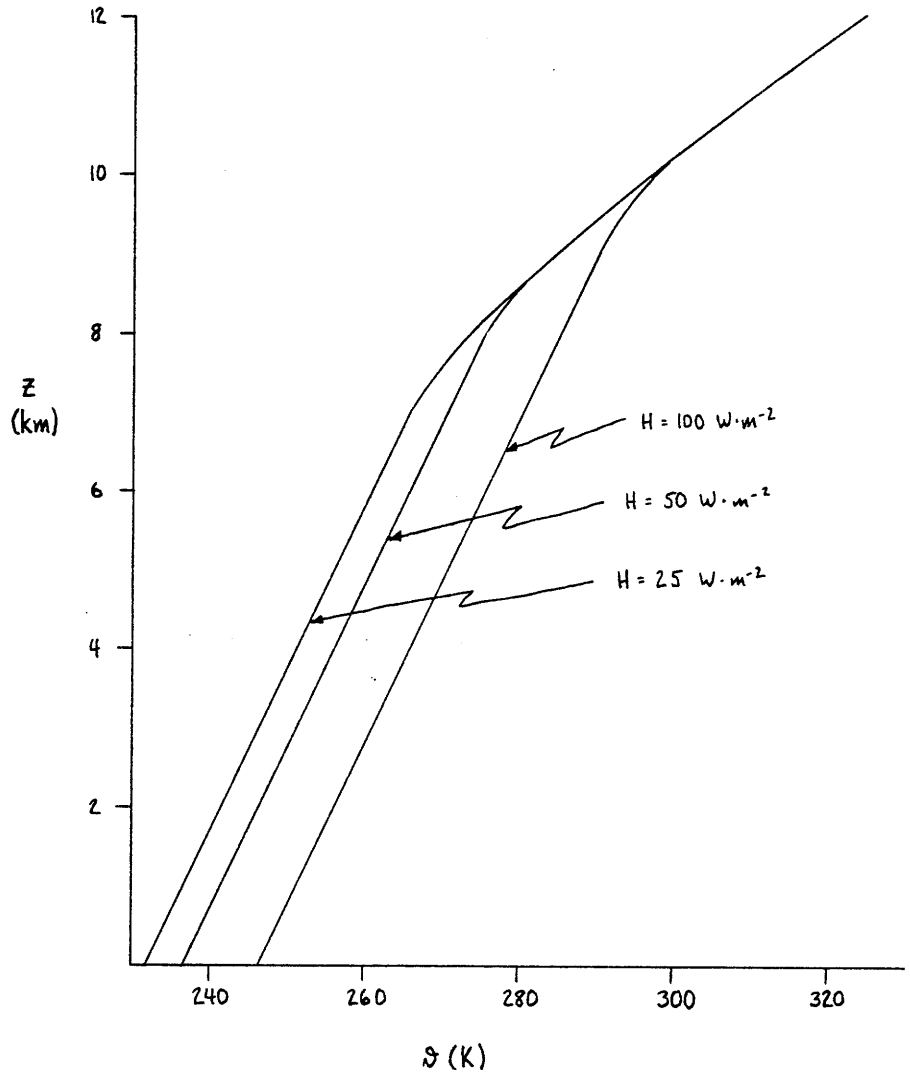

Figure 3.1.4 The RCE solution of the present model computed with the critical lapse rate of Manabe and Weatherald for different values of H, the surface heat flux with τ = 30 days.

the results in a qualitative, rather than a strictly quantitative, manner.

As was pointed out in the introduction, Manabe and Weatherald's RCE model was not a true radiative-convective equilibrium model since it took 4.9 K km^{-1} rather than 0 K km^{-1} as the critical potential temperature lapse rate below which convection would occur. As a basis with which to compare the RDE profiles to be discussed later, we want RCE profiles in which a neutral lapse rate is the critical rate. These are shown in figures 3.1.5 (for various values of H with $\tau = 30$ days) and 3.1.6 (for various values of τ with $H=50$ W m^{-2}). The variation of the profiles with the surface heat flux is similar to that of figure 3.1.4. In figure 3.1.6 we see, as expected, that, as the radiative time constant decreases, the radiative cooling of the lower atmosphere increases and the profile tends to look more like the radiative equilibrium profile.

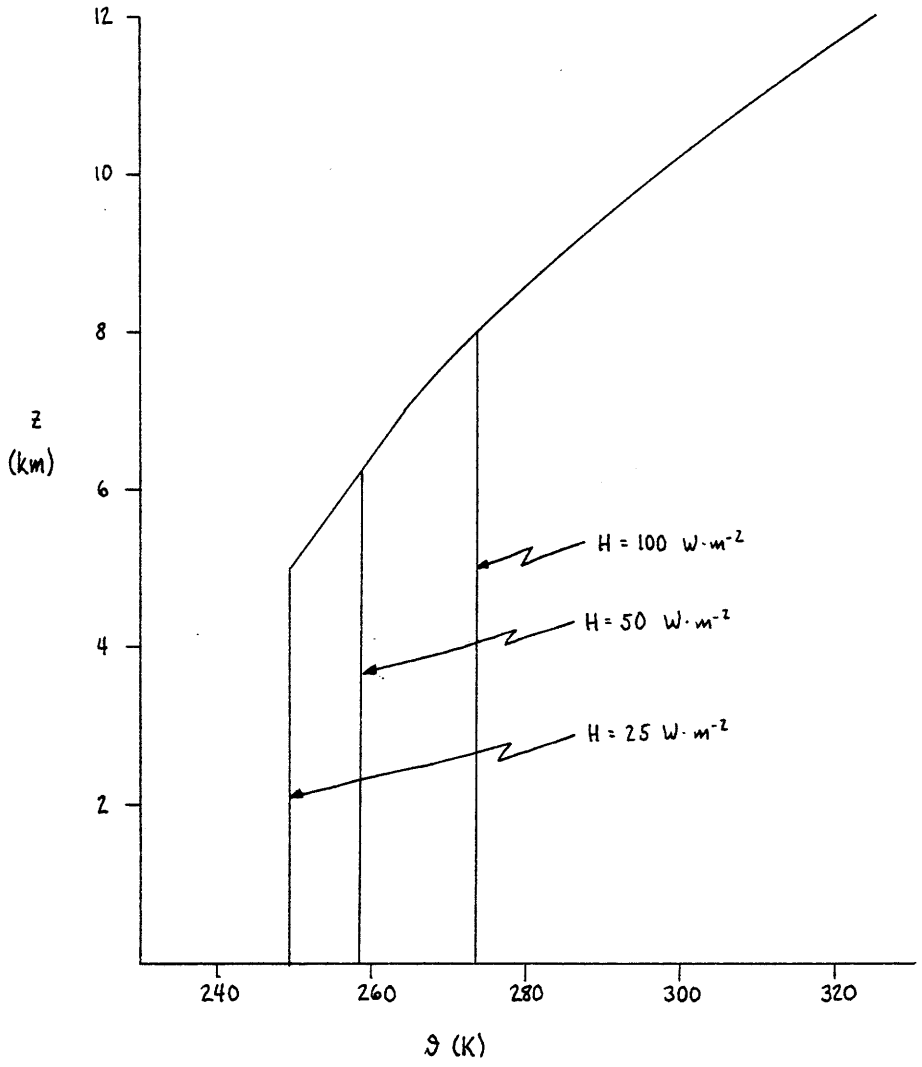

Figure 3.1.5 RCE solutions of the model for various values of the surface heat flux with τ = 30 days.

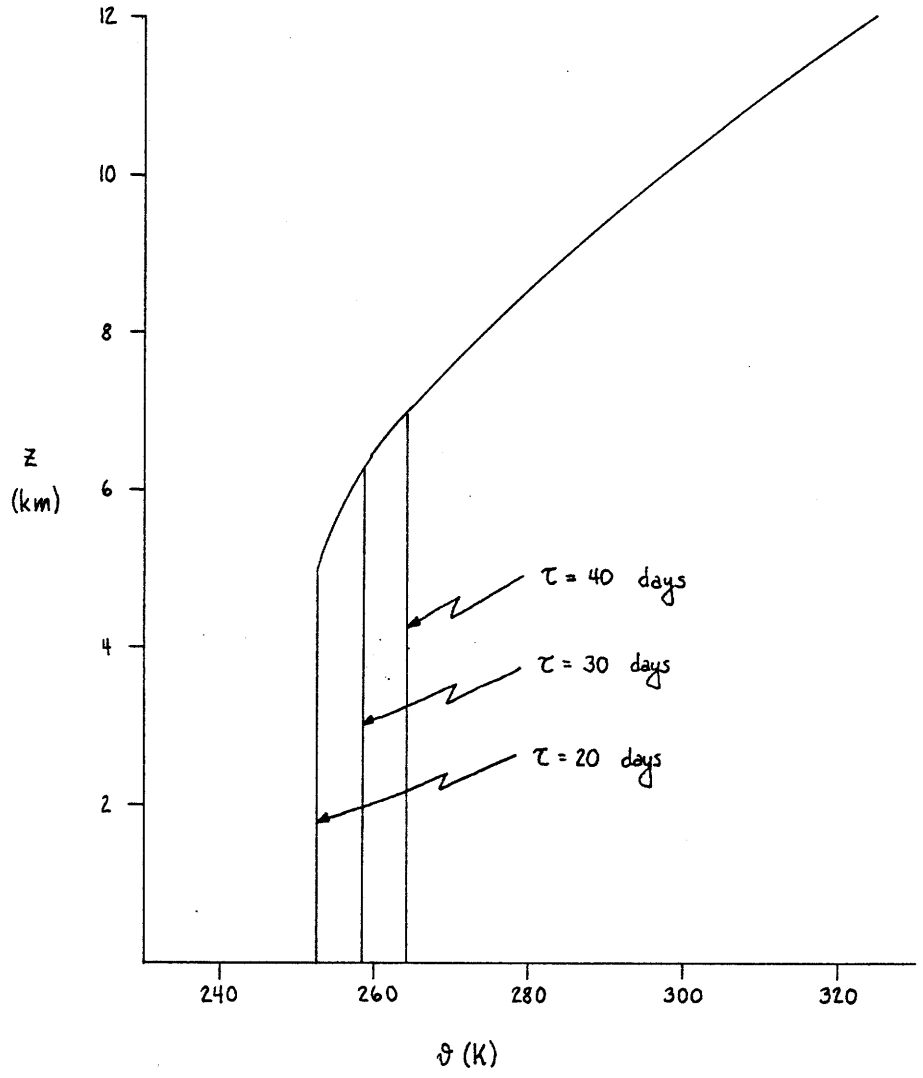

Figure 3.1.6 RCE solutions of the model for various values of the radiative time constant, τ , with H = 50 W m^{-2}.

3.2 Radiative-Dynamical Equilibrium

The radiative-convective profiles of figures 3.1.5 and 3.1.6 are the first order approximations to the vertical temperature structure of the atmosphere and, as such, will be used as the initial state in our calculations of the second order approximation, the radiative-dynamical equilibrium state. The RDE calculations will be carried out for baroclinic eddies of three different wavelengths, zonal wavenumbers 3,6, and 9, as well as for various values of the radiative time constant and surface heat flux. Zonal wavenumber 3 corresponds to the very long planetary scale waves, wavenumber 6 is the wavenumber of maximum instability of the zonal flow, and wavenumber 9 will be used to represent the short surface-trapped cyclones; with these three values we thus cover the range of scales of baroclinic eddies fairly well (though, for reasons which will be clear later, we have not included the surface-trapped waves of wavenumber 12-15).

Figure 3.2.1 shows the RDE profile (solid line) for the "best value" or control case with $k_\ell = 6$, $\tau = 30$ days, and $H = 50$ W m^{-2}, as well as the corresponding RCE profile (dashed line). We see that above 12 kilometers the profile does not differ from the radiative-convective profile while below this the RCE profile has been modified by the baroclinic eddies. In particular, the eddies have cooled the lowest 4 kilometers of the troposphere and heated the region between 4 and 12 kilometers, the net result being that the lower troposphere has been stabilized. Thus in RCE convection occurs in the lowest 6 kilometers of the atmosphere, leading to a neutral lapse rate there, whereas in RDE this region has an

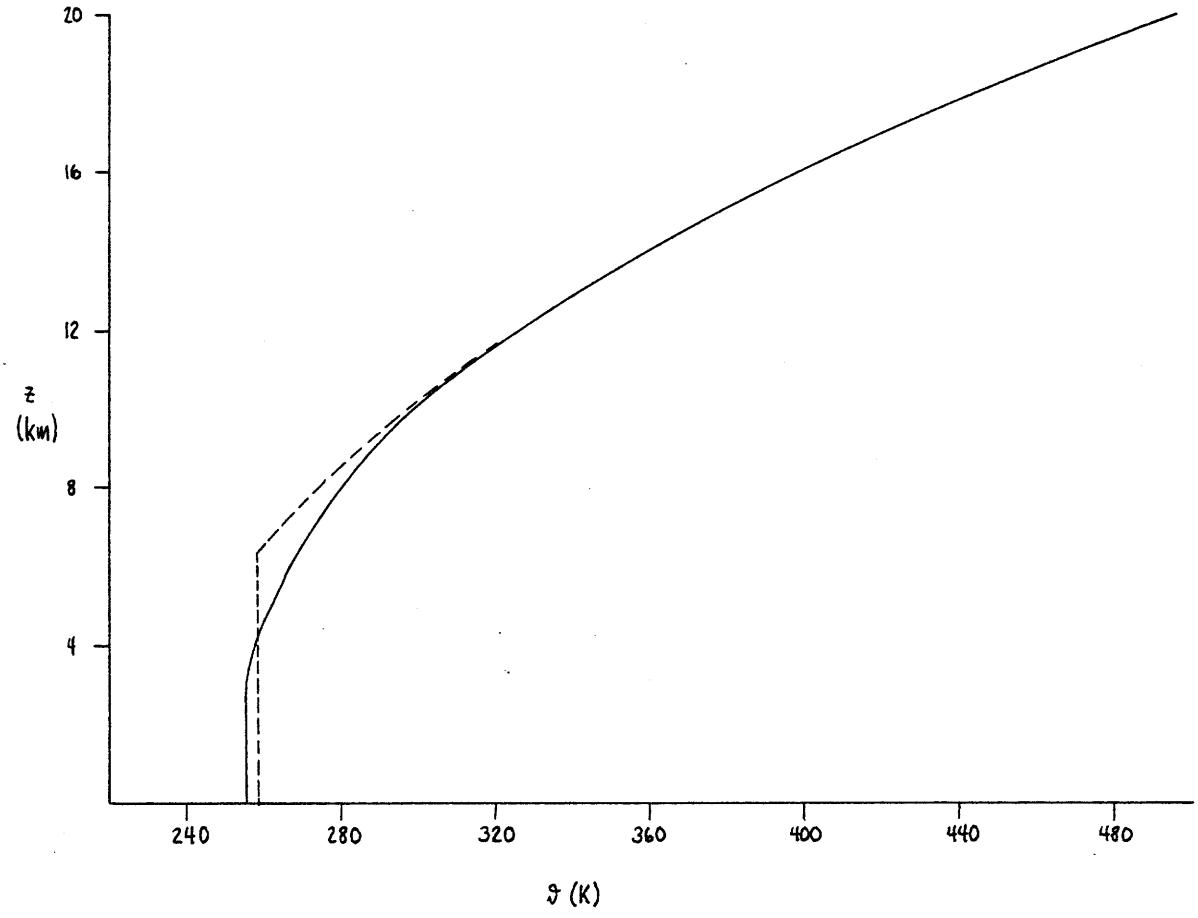

Figure 3.2.1 The RDE solution for $k_z = 6$, $\tau = 30$ days, and $H = 50$ W m^{-2} (solid line) and the corresponding RCE state (dashed line).

average stability of 1.6 K km^{-1}. To see how the eddy does this, we refer to figure 3.2.2, which shows the vertical heat flux, $\rho c_p \langle \overline{\omega\vartheta} \rangle$, of the eddy as a function of height. The heating due to this flux is $-\rho c_p \frac{\partial}{\partial z} \langle \overline{\omega\vartheta} \rangle$, so we see that below 3 kilometers the eddy is cooling the atmosphere and between 3 and 12 kilometers it is warming the atmosphere.

The variation of the RDE profile with the surface heat flux and with the radiative time constant is shown in figures 3.2.3 and 3.2.4. Increasing the surface heat flux, H, tends to warm and destabilize the lower troposphere, so that, for example, the H = 100 W m^{-2} profile is warmer and has a deeper convecting region than the H = 50 W m^{-2} profile. Corresponding to this change in the vertical temperature structure there is a change in the structure of the eddies, as can be seen in figures 3.2.5, 3.2.6, and3.2.2 (for H = 50 W m^{-2}). What we see is that the eddies tend to be concentrated near the regions of low stability, so that the maximum vertical heat flux of the eddy of figure 3.2.5 is depressed relative to the maximum vertical heat flux of the eddy of figure 3.2.2, and the maximum of figure 3.2.6. is higher than that of figure 3.2.2. Since the magnitude of the maximum eddy flux is essentially the same in each of the three cases the heating and cooling by the eddies, being proportional to $-\frac{\partial}{\partial z} \langle \overline{\omega\vartheta} \rangle$, is greater for the small scale eddies of figure 3.2.5 than for the larger scale eddies of figure 3.2.6, which is evident when we compare the RDE profiles of figure 3.2.3 with their corresponding RCE profiles (dashed lines). The same sort of discussion is applicable to the profiles for various values of the radiative time constant shown in figure 3.2.6

Finally, in figure 3.2.7 we show the RDE profiles produced by the

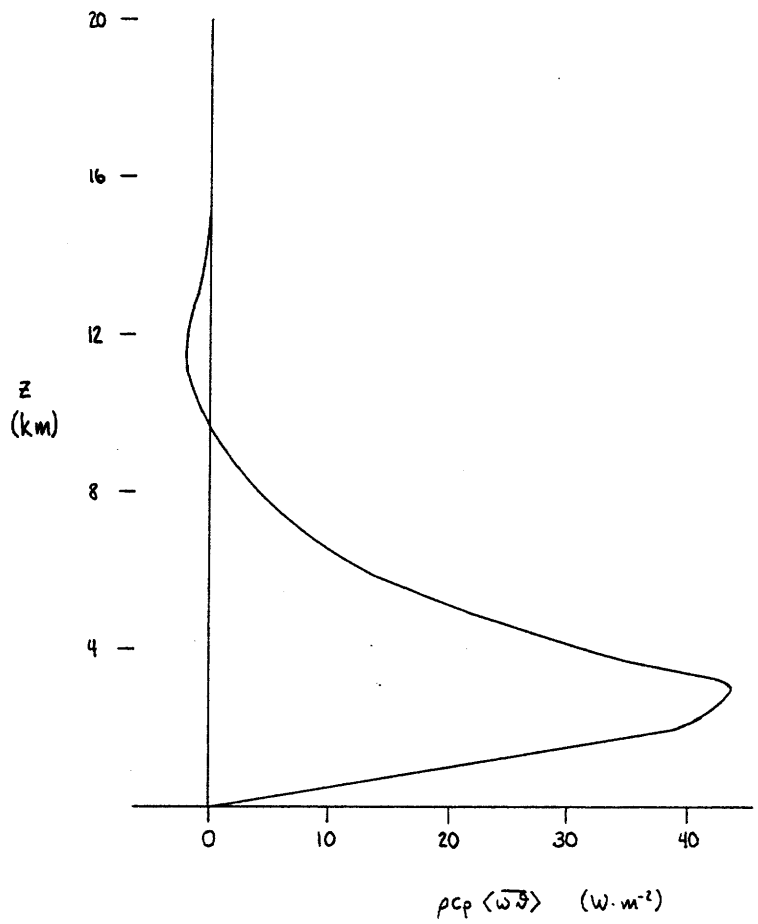

Figure 3.2.2 The eddy heat flux, $\rho c_p \langle \overline{\omega}\overline{\vartheta} \rangle$, for the $k_z = 6$ wave with $\tau = 30$ days and $H = 50$ W m^{-2} (see figure 3.2.1).

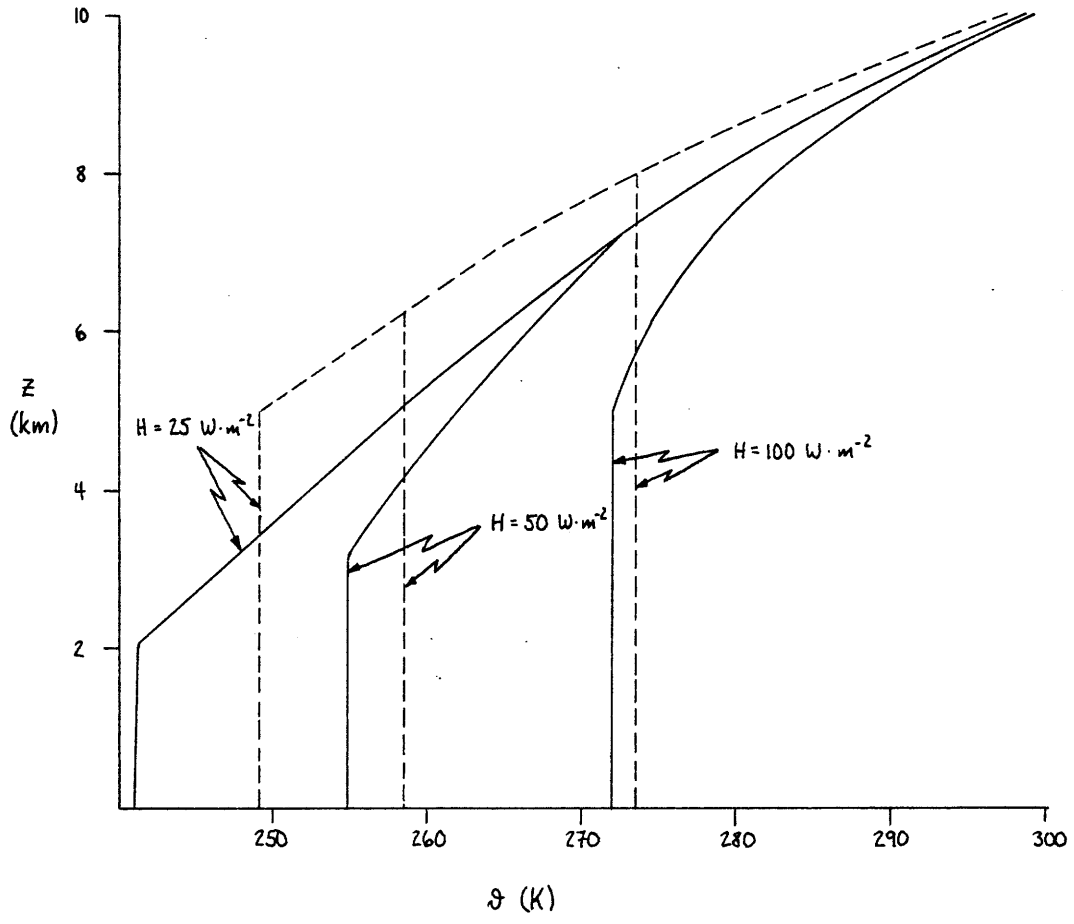

Figure 3.2.3 RDE solutions (solid lines) for the $k_z = 6$ wave with $\tau = 30$ days and various values of the surface heat flux, H, and the corresponding RCE states (dashed lines).

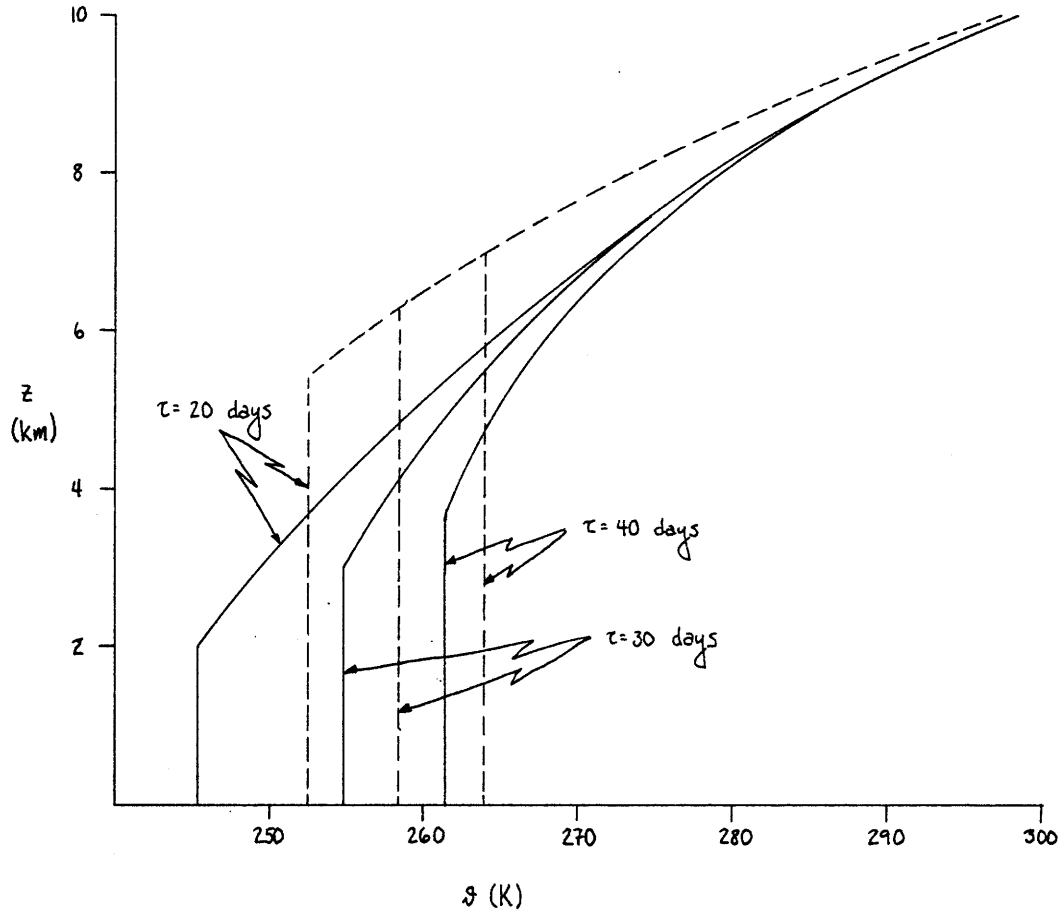

Figure 3.2.4 RDE states (solid lines) for the $k_z = 6$ wave for H = 50 W m^{-2} and various values of the radiative time constant τ, and the corresponding RCE states (dashed lines).

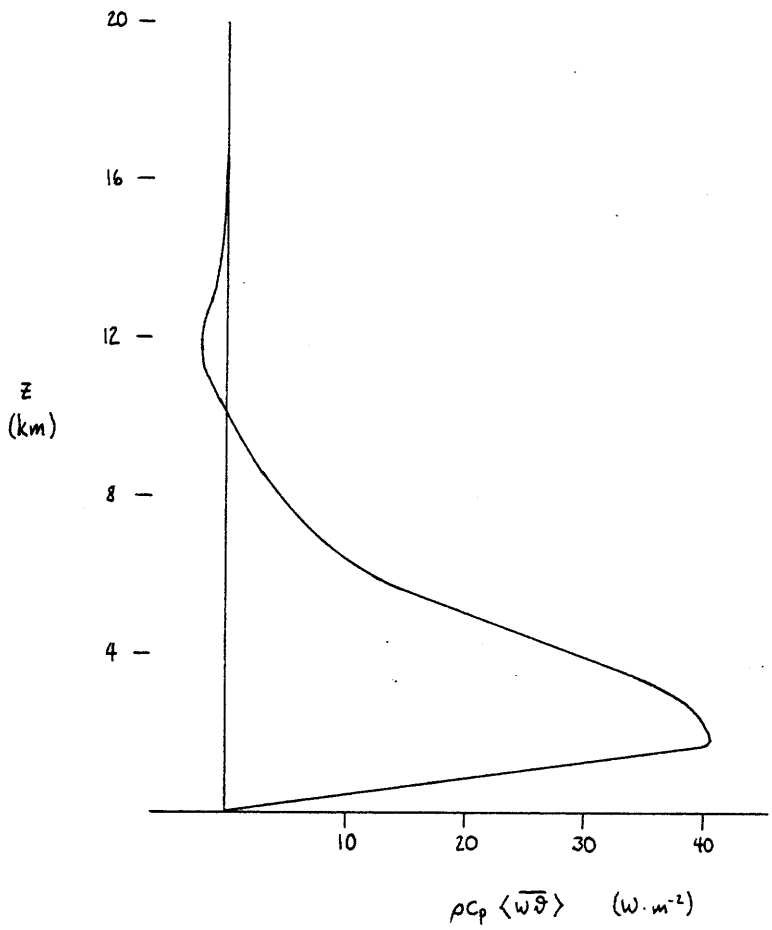

Figure 3.2.5 The eddy heat flux, $\rho c_p \langle \overline{w\vartheta} \rangle$, for the $k_z = 6$ wave with $\tau = 30$ days and $H = 25$ W m^{-2}.

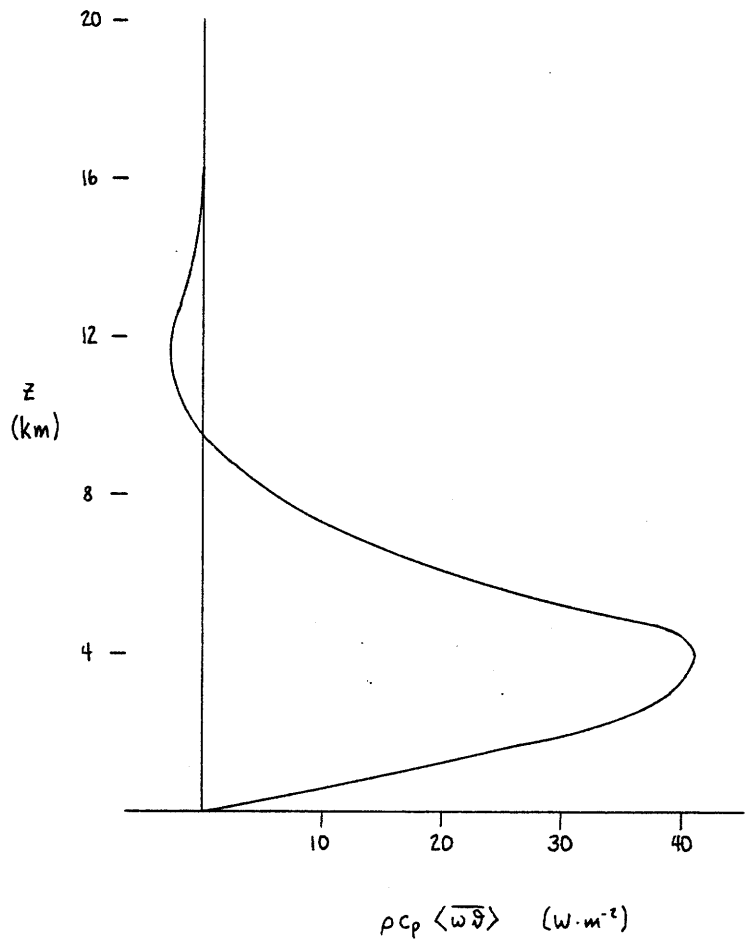

Figure 3.2.6 The eddy heat flux, $\rho c_p \langle \overline{\omega \vartheta} \rangle$, for the $k_z = 6$ wave with $\tau = 30$ days and $H = 100$ W m^{-2}.

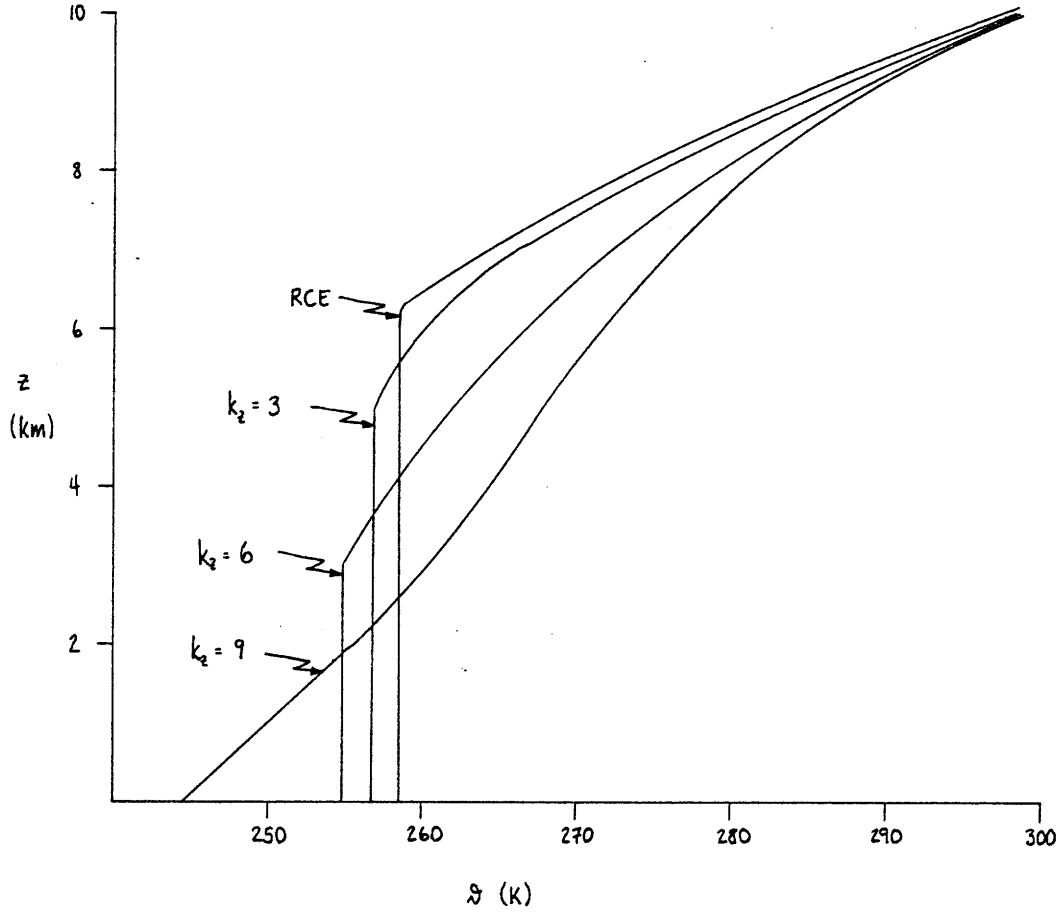

Figure 3.2.7 The RCE state and RDE states for various values of the zonal wavelength k_z for τ = 30 days and H = 50 W m^{-2}.

three different scales of eddies when $\tau = 30$ days and $H = 50\ W m^{-2}$. We see that the profile produced by the eddy of zonal wavenumber 3 differs very little from the RCE profile while the profile for wavenumber 9 is considerably more stable than RCE. For the wavenumber 9 profile there is, infact, no convecting region which is resolvable by the one kilometer grid employed in these calculations. As before, the differences in the equilibrium profiles can be understood by examining the heat fluxes due to the eddies, shown in figures 3.2.8, 3.2.9, and 3.2.1 (for $k_z = 6$). We see here that a low wavenumber eddy has a large vertical scale while a higher wavenumber corresponds to a smaller vertical scale. Since the RCE state of each of the eddies is the same, this variation of the vertical scale is not, as in the previous cases, due to the eddy being trapped in the region of low static stability; what is operating here is the tendency for geostrophic disturbances such as the eddies under discussion to maintain a constant aspect ratio . Thus, if L_x is the zonal scale and L_z the vertical scale of the eddy, the two are related approximately by $\frac{L_x}{L_z} \sim \frac{N}{f}$ where N is the Brunt-Väisälä frequency and f the Coriolis parameter. This constant aspect ratio is the reason that higher wavenumber eddies such as $k_z = 12$ and $k_z = 15$ were not included in this study: their vertical scales would be even smaller than that of the $k_z = 9$ eddy and could not be adequately resolved by our one kilometer grid spacing.

Assuming the fluxes of the various eddies to be of the same order of magnitude, this relation between the vertical & horizontal scales would imply that the low wavenumber eddies, haveing large vertical scales, would do less heating and cooling than high wavenumber eddies with samll

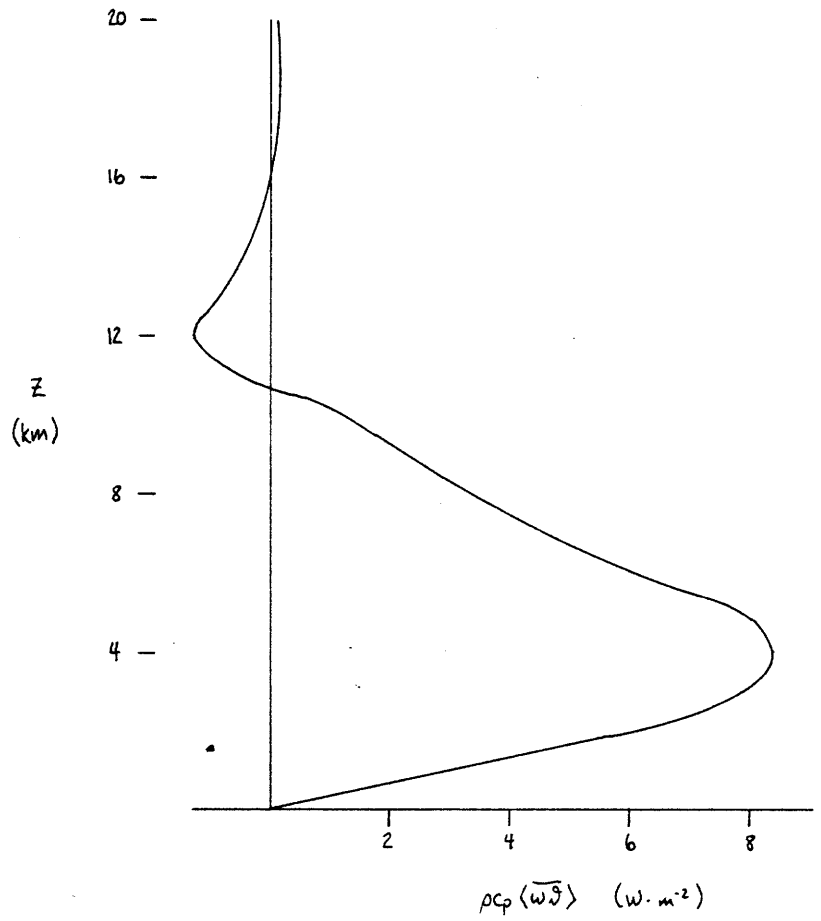

Figure 3.2.8 The eddy heat flux for the $k_z = 3$ wave with $\tau = 30$ days and $H = 50$ W m^{-2}.

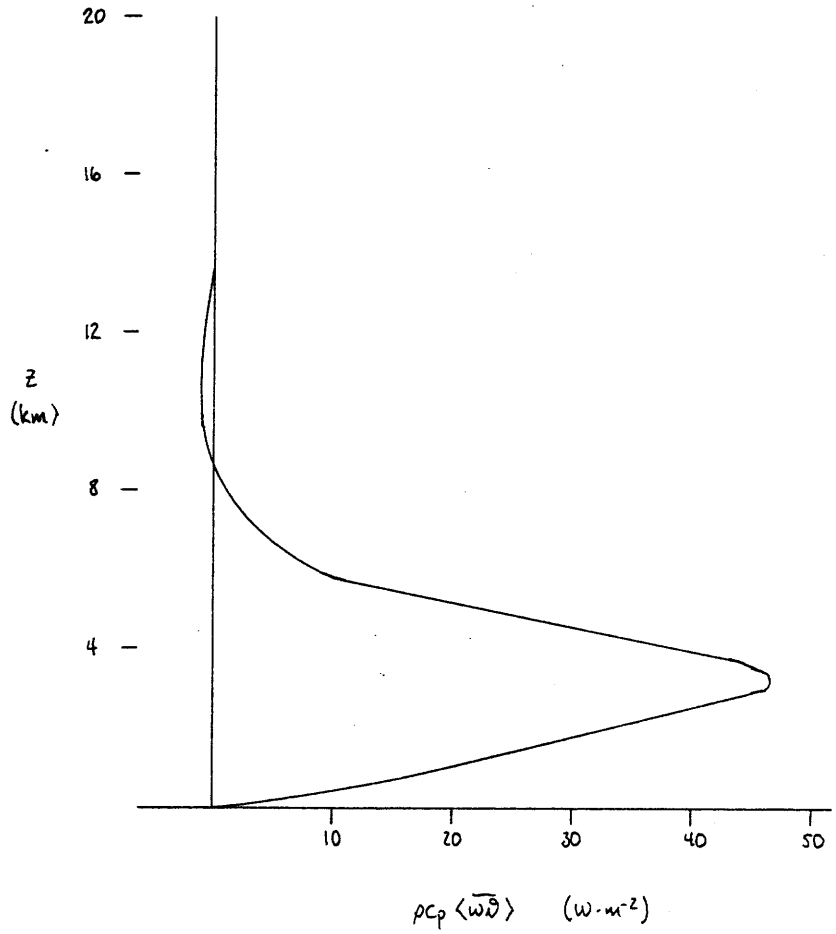

Figure 3.2.9 The eddy heat flux for the $k_z = 9$ wave with $\tau = 30$ days and $H = 50$ W m^{-2}.

vertical scales. In the present case this difference is enhanced by the fact that the magnitude of the heat flux of the small scale eddies is greater than that of the large scale eddies: because of our amplitude condition (equation 2.2.10), small scale eddies must be much more vigorous than large scale onesin order to have a total kinetic energy equal to that of the mean flow.

One very interesting feature of the $k_z = 9$ profile is that,due to the strong cooling by the eddy heat flux, the lowest 3 kilometers of the atmosphere are actually more stable than the atmosphere directly above them. This is also true of the real atmosphere as observed by Oort and Rasmusson (1971), whose data for the annual average potential temperature at 45°N is plotted with the profile for $k_z = 9$ in figure 3.2.10. Except for the shift of the $k_z = 9$ profile towards the cold end of the graph, the two profiles are virtually identical below 13 km. While, because of the deficiencies of our model, this correspondence must be considered purely fortuitous, the qualitative similarity of the two profiles suggests that it is the short wavelength eddies which play the major role in determining the stability of the troposphere.

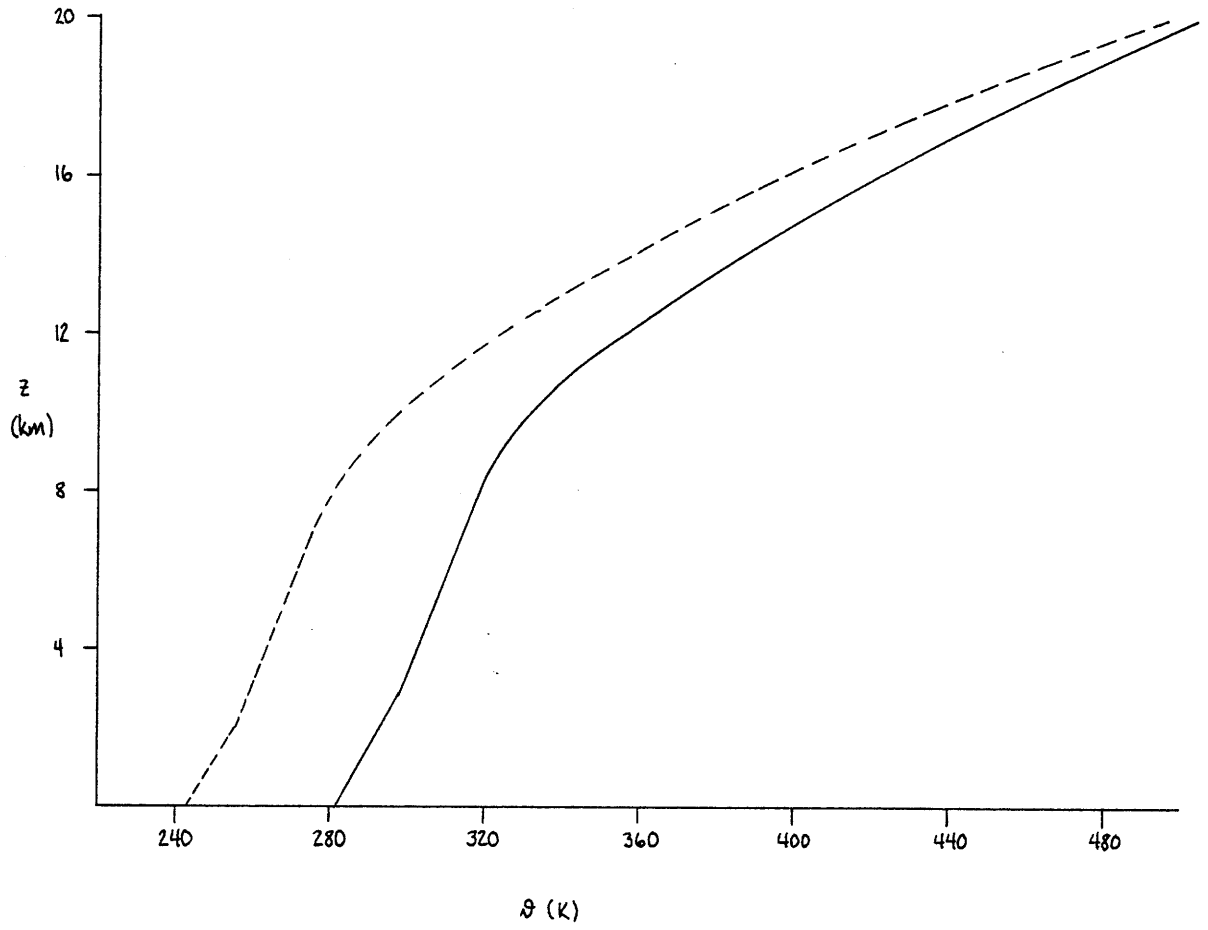

Figure 3.2.10 Observed annual average potential temperature at 45° N latitude from Oort and Rasmusson (1971) (solid line) and the RDE solution of the model for $k_z = 9$, $\tau = 30$ days, and $H = 50$ W m^{-2} (dashed line).

4. Conclusion

4.1 Discussion of Results

Despite some deficiencies in our model, the results obtained in the previous chapter provide us with some idea of how the mean static stability of the mid-latitude troposphere is maintained. That the temperature structure cannot be due to a radiative-dry convective balance was mentioned in the introduction. As was pointed out then, and as can be seen from figures 3.1.5 and 3.1.6, these processes can only lead to a convecting region (with neutral stability) underneath a region in radiative equilibrium; since dry convection cannot transport heat against a temperature gradient, it is impossible for it to produce a stable temperature profile. Baroclinic eddies, however, can transport heat upward in a statically stable atmosphere and are thus possible candidates for maintaining the observed temperature structure. The purpose of this paper is to find out how well these eddies can account for the observed temperature profile.

In discussing the model results, we distinguish between two types of equilibrium state: radiative-convective-dynamical equilibrium (RCDE) and radiative-dynamical equilibrium (RDE) The RCDE states are characterized by three regions (see figure 4.1.1): a convective region several kilometers deep in which dry convection is the dominant process, a dynamical region from the top of the convective region to about 10 to 12 kilometers in which baroclinic eddies play the major role, and above these regions, a region in which the atmosphere is in radiative equilibrium.

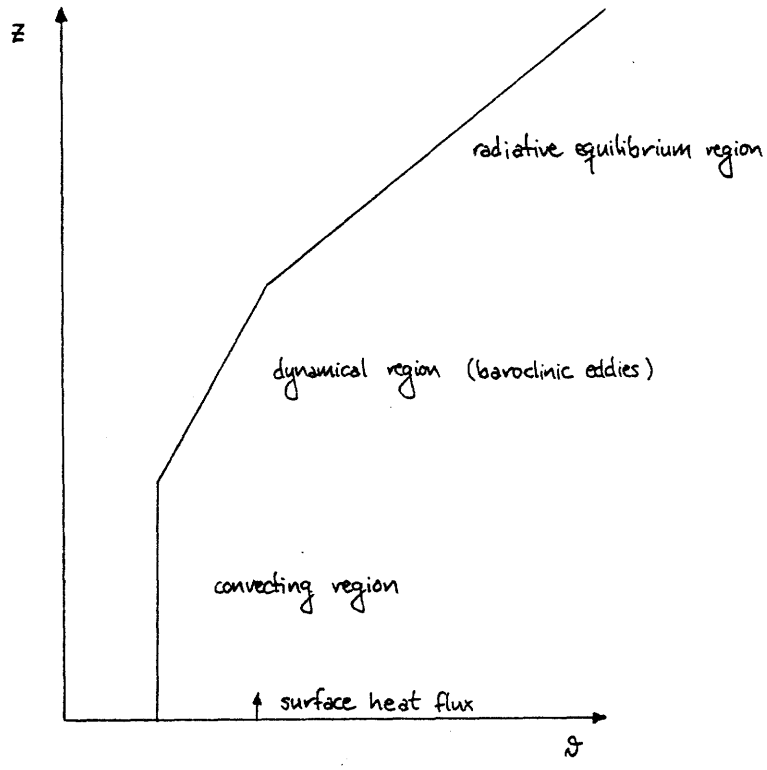

Figure 4.1.1 Schematic diagram of the radiative - convective - dynamical equilibrium state.

The equilibrium states for baroclinic waves of zonal wavenumber 3 and 6 (figure 3.2.7) fall into this RCDE catagory. Due to their large horizontal scale, these eddies also have a fairly large vertical scale, and consequently the cooling by the eddies in the lower atmosphere is not enough to offset the sensible heat flux from the ground. Thus the surface heat flux destabilizes the lower atmosphere and the convecting region is formed.

For baroclinic waves of small horizontal scale (the $k_\ell = 9$ eddy of figure 3.2.9, for example) , the vertical scale is correspondingly small and the cooling near the ground correspondingly large. These eddies are thus able to overcome the destabilizing surface heat flux and keep the atmosphere near the ground stable, leading to the RDE profile of figure 4.1.2. Because of the stabilization of the lower atmosphere by the small eddies this profile lacks the convective region of the RCDE case and the dynamical region reaches all the way to the surface.

The observed atmosphere (figure 3.2.10) clearly lacks the convecting region of the RCDE states; in fact near the ground where we would expect to find the convecting region, the atmosphere is actually more stable than it is higher up. This is exactly what we see in the RDE state produced by the zonal wavenumber 9 eddy (figure 3.2.10); for this wave, the cooling near the ground is so strong that it more than offsets the surface heat flux and actually stabilizes the atmosphere. While the RDE state of the wavenumber 9 eddy is significanly cooler than the observed profile, the qualitative similarity between the two suggests that the static stability of the real atmosphere in mid-latitudes is maintained by the dynamical heat fluxes of small scale baroclinic waves. There is

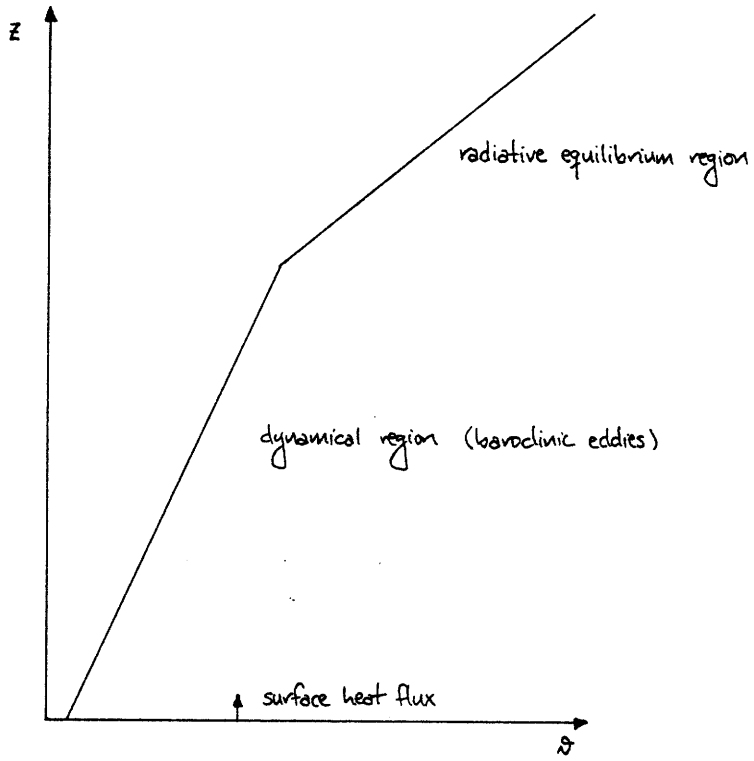

Figure 4.1.2 Schematic diagram of the radiative - dynamical equilibrium state.

an ample supply of such eddies to do this: at 45°N, zonal wavenumber 9 corresponds to a wavelength of about 3000 kilometers, a typical scale for the cyclones which produce much of our weather. (See Palmén and Newton, 1969, figure 6.10 for such a wavenumber 9 case.)

In conclusion, it should be pointed out that we are in no way making the claim that dry convection does not occur in the atmosphere. The mean temperature structure of the atmosphere is by no means observed everywhere at every time: there are many situations in which convection does occur and in which it is an important mechanism for transporting heat. What we have tried to do in this paper is show that the explanation of the mean vertical temperature structure of the mid-latitude tropopause does not require the invocation of dry convection, as is often done, but can be adequately accounted for in terms of a balance between radiative heat fluxes and the heat fluxes due to baroclinic eddies. While a number of deficiencies in the present model prohibit us from claiming that this contention has been demonstrated to be true, the results obtained tend to lend support to the hypothesis. Hopefully future models, free of the shortcomings of the present one, will clarify the matter.

4.2 Suggestions for further research

One of the major shortcomings of the model used in the preceeding work is that it does not include latent heat fluxes, which are a very important source of heat transport in the real atmosphere. In particular, the surface heat flux of the present model would be increased considerably if latent heat fluxes were included. Inclusion of latent heat fluxes in the model would require a parameterization of the release of this heat by condensation, and while this would not be too difficult an addition there was not adequate time in which to do it for this paper.

Another shortcoming of the present model was pointed out by P. H. Stone as the work was drawing to a close: namely that the radiative equilibrium profile used in the model is not the appropriate one for the purpose of the model. The RE profile used is the profile computed by Manabe and Weatherald for an atmosphere with a fixed distribuiton of relative himidity This is the true RE profile, i.e. the one which would occur if there were no dynamics in the atmosphere. In a model such as ours, however, dynamics is assumed to play an important role, and the temperature and humidity profiles will not be too much different from the observed profiles. In this case the appropriate RE profile to use is that of Manabe and Strickler (1964) in which the observed distribution of absolute humidity is used in the computation. The profile thus obtained is shown in figure 4.2.1 and is seen to be considerably different from the profile of Manabe and Weatherald (figure 3.1.1).

Finally, the present model suffers from limited resolution in the vertical. With a one kilometer vertical grid it is just possible to

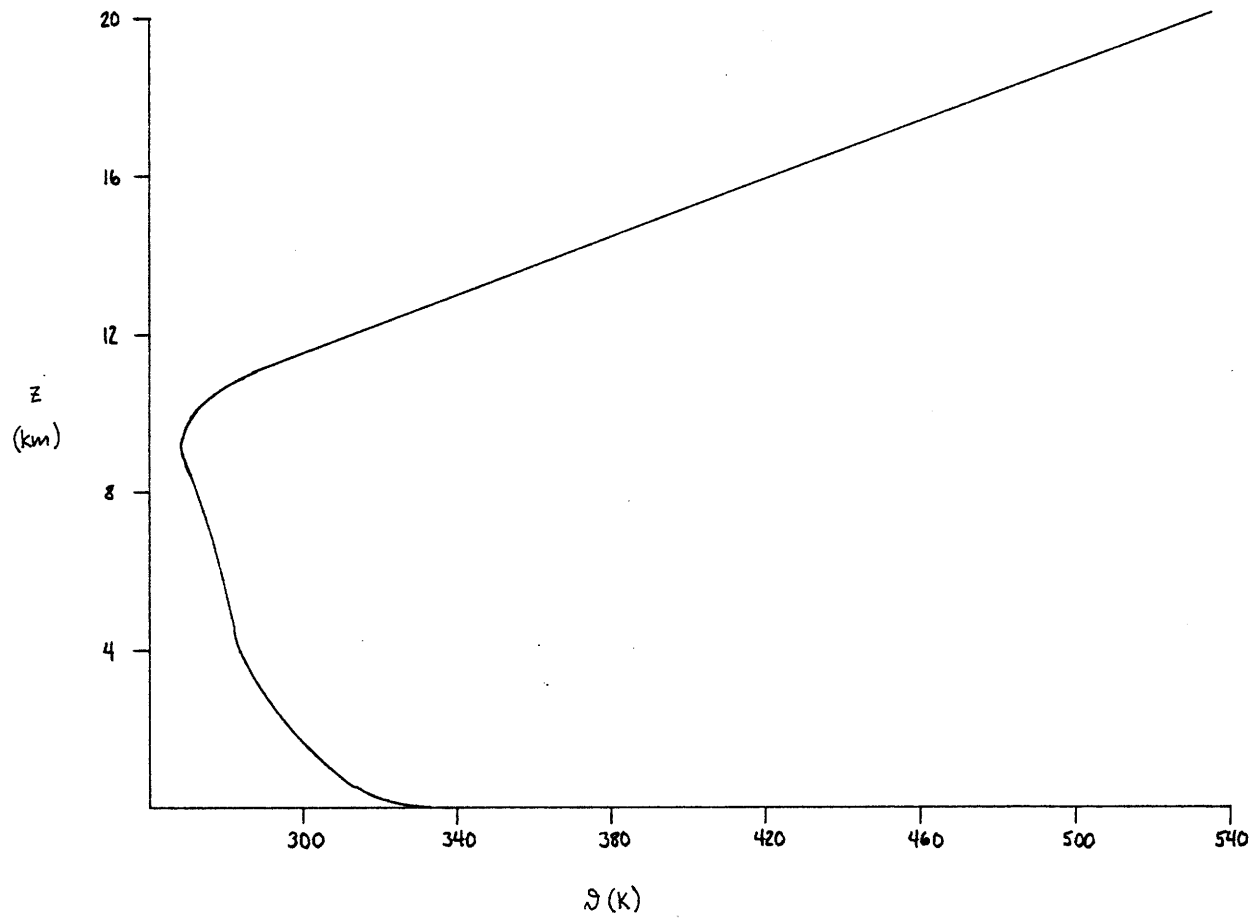

Figure 4.2.1 Radiative equilibrium potential temperature profile computed for a fixed distribution of absolute humidity. From Manabe and Strickler (1964).

adequately represent the vertical structure of the $k_z=9$ wave of figure 3.2.9: higher wavenumber eddies cannot be represented well at all. An attempt was made to run the model with double the present resolution, but difficulties were encountered in solving the eigenvalue polynomial (equation A.7) for the phase speed of the baroclinic wave, as doubling the resolution doubles the order of the polynomial. Solving a high order polynomial with complex coefficients for its complex roots in an efficient manner (time is important, as a typical run requires solveing for the roots at each of $\sim$ 2000 timesteps) is somewhat touchy, but by no means impossible. One possibility for avoiding polynomials of too high an order would be a variable grid, with fine resolution near the ground where we want to resolve the eddy structure and coarser resolution higher up where the main processes are radiative.

It is hoped that someone will, in the future, correct the deficiencies mentioned above and thus clarify the role of baroclinic eddies in maintaining the static stability of the mid latitude troposphere; it is an aspect of mid-latitude atmospheric dynamics which, despite the efforts of the present paper, has received too little attention to date.

APPENDIX A: Solution of the Eigenvalue Problem

The eigenvalue problem which we wish to solve is that of equation 2.2.6, i.e.

$$f^2 \omega_{zz} - \frac{2f^2 \bar{u}_z}{c+\bar{u}} \omega_z - \alpha g k^2 \bar{\vartheta}_z \omega = 0 \qquad (A.1)$$

subject to the boundary conditions that $\omega = 0$ at $z = 0, h$.

To solve this numerically, the variables are assumed to be known at N levels in the atmosphere, $z = z_1, z_2, \cdots z_N$ where $z_i = i \cdot \Delta$.

The derivatives in equation A.1 are then written in centered finite difference form:

$$\left(\frac{d\omega}{dz}\right)_i = \frac{1}{2\Delta}\left(\omega_{i+1} - \omega_{i-1}\right)$$

and

$$\left(\frac{d^2\omega}{dz^2}\right) = \frac{1}{\Delta^2}\left(\omega_{i+1} - 2\omega_i + \omega_{i-1}\right)$$

When these are substituted into equation A.1 and the terms are rearranged, one gets the equation

$$A_i \omega_{i+1} + B_i \omega_i + C_i \omega_{i-1} = 0 \qquad (A.2)$$

where

$$A_i = f^2(c+\bar{u}_i) - \bar{u}_{zi} f^2 \Delta \tag{A.3}$$

$$B_i = -(2f^2 + \alpha g k^2 \Delta^2 \bar{\vartheta}_{zi})(c+\bar{u}_i) \tag{A.4}$$

and

$$C_i = f^2(c+\bar{u}_i) + \bar{u}_{zi} f^2 \Delta \tag{A.5}$$

Writing equation A.2 for $i=1,N$ and remembering the boundary conditions $\omega_0=0$ and $\omega_{N+1}=0$, we get a set of algebraic equations which can be written as a tridiagonal matrix equation:

$$\begin{pmatrix} B_1 & A_1 & \cdots & 0 \\ C_2 & B_2 & A_2 & \\ & C_3 & B_3 & A_3 \\ & & \ddots & \ddots \\ & & C_{N-1} & B_{N-1} & A_{N-1} \\ 0 & \cdots & & C_N & B_N \end{pmatrix} \begin{pmatrix} \omega_1 \\ \omega_2 \\ \omega_3 \\ \vdots \\ \omega_{N-1} \\ \omega_N \end{pmatrix} = 0 \tag{A.6}$$

In order for this equation to hold for a given value of k, the determinant of the matrix must vanish. Expanding this determinant gives a polynomial of order N in c, $p_N(c)$, which can be computed by the recursion relation

$$p_{-1} = 0$$

$$p_0 = 1$$

$$p_i = B_i p_{i-1} - A_{i-1} C_i p_{i-2} \qquad i = 1, N$$

The zeros of $p_N(c)$ are the phase speeds of the $N/2$ pairs of growing and damped baroclinic modes. Newton's method was used to find these roots, but as this method is very temperamental in the complex plane, especially with polynomials of as high an order as ours, a fairly good initial guess for the root is needed. If the initial temperature profile in the model is linear, we may use Stone's (1966) model to get a good guess for the phase speed during the first timestep. Once we have the root for one timestep this root is usually an adequate guess for the root in the next timestep, but if the initial profile is not linear or if a root is not a good guess for the succeeding timestep, we must obtain a guess by other means. In this case LSQNK2 , a subroutine developed at MIT to find zeros of functions by employing some techniques from complex analysis, was used. This is a much more certain way to find roots, but because it is also very slow (taking 5 to 30 seconds to find one root), its use was limited to those cases which Newton's method could not handle. Once the phase speed, c , of the desired baroclinic mode is found it is put back into the expressions for the coefficients A_i, B_i, and C_i (equations A.3, A.4, and A.5) giving numerical values for these. Then Richtmyer's "double sweep" method (Richtmyer and Morton, 1967, pg. 200) is used to compute the vertical velocities, $\omega_1, \omega_2, \ldots, \omega_N$, at the N levels from equation A.6.

APPENDIX B: The Crank-Nicholson Scheme

The Crank-Nicholson time differencing scheme is an implicit scheme-that is, in an equation of the form $\frac{dx}{dt} = f(x)$, it uses the predicted value of x , as well as its past value, in the evaluation of $f(x)$. While this makes the scheme rather complicated computationally, it also frees it from the numerical instabilities encountered with, say, the leap-frog method. The equation for which we wish to use this scheme is equation 2.3.2:

$$\frac{\partial}{\partial t}\langle\bar{\vartheta}\rangle = -\frac{\partial}{\partial z}\mu\frac{\partial}{\partial z}\langle\bar{\vartheta}\rangle + \frac{\partial F}{\partial z} + \frac{1}{\tau}\left[\langle\bar{\vartheta}_e\rangle - \langle\bar{\vartheta}\rangle\right] \qquad \text{(B.1)}$$

where

$$\mu = \frac{c_i|A|^2}{2}\frac{|\omega|^2}{k|c+\bar{u}|^2}$$

and

$$F = \frac{m|A|^2}{2k}\,\mathrm{Re}\left(\frac{i\omega^* v}{c+\bar{u}}\right).$$

Writing the last two terms of equation B.1 as

$$E_j^n = \left(\frac{\partial F}{\partial z}\right)_j^n + \frac{1}{\tau}\left[\langle\bar{\vartheta}_e\rangle_j - \langle\bar{\vartheta}\rangle_j^n\right],$$

letting the symbol $(\delta\vartheta)_j^n$ denote the finite space difference centered at level j at the n^{th} timestep, and dropping the angle brackets and overbars for notational ease, we write equation B.1 as

$$\frac{1}{\Delta t}\left(\vartheta_j^{n+1} - \vartheta_j^{n}\right) = -\frac{1}{2\Delta^2}\left\{\left[\delta\left(\mu\delta\vartheta\right)\right]_j^{n+1} + \left[\delta\left(\mu\delta\vartheta\right)\right]_j^{n}\right\} + \epsilon_j^{n}$$

$$= -\frac{1}{2\Delta^2}\left\{\left[\mu_{j+\frac{1}{2}}\left(\vartheta_{j+1}^{n+1} - \vartheta_j^{n+1}\right) - \mu_{j-\frac{1}{2}}\left(\vartheta_j^{n+1} - \vartheta_{j-1}^{n+1}\right)\right]\right.$$

$$\left. + \left[\mu_{j+\frac{1}{2}}\left(\vartheta_{j+1}^{n} - \vartheta_j^{n}\right) - \mu_{j-\frac{1}{2}}\left(\vartheta_j^{n} - \vartheta_{j-1}^{n}\right)\right]\right\} + \epsilon_j^{n}$$

where $\mu_{j+\frac{1}{2}} = \frac{1}{2}\left(\mu_j + \mu_{j+1}\right)$. Rearranging these terms gives the equation

$$\beta_{j+\frac{1}{2}}\,\vartheta_{j+1}^{n+1} + \left(1 - \beta_{j+\frac{1}{2}} - \beta_{j-\frac{1}{2}}\right)\vartheta_j^{n+1} + \beta_{j-\frac{1}{2}}\,\vartheta_{j-1}^{n+1} \qquad \text{(B.2)}$$

$$= -\beta_{j+\frac{1}{2}}\,\vartheta_{j+1}^{n} + \left(1 + \beta_{j+\frac{1}{2}} + \beta_{j-\frac{1}{2}}\right)\vartheta_j^{n} - \beta_{j-\frac{1}{2}}\,\vartheta_{j-1}^{n} + \Delta t\,\epsilon_j^{n}$$

where $\beta_j = \mu_j\,\Delta t / (2\Delta^2)$. Writing

$$A_j = \beta_{j+\frac{1}{2}}$$

$$B_j = 1 - \beta_{j+\frac{1}{2}} - \beta_{j-\frac{1}{2}}$$

$$C_j = \beta_{j-\frac{1}{2}}$$

$$D_j = -\beta_{j+\frac{1}{2}}\,\vartheta_{j+1}^{n} + \left(1 + \beta_{j+\frac{1}{2}} + \beta_{j-\frac{1}{2}}\right)\vartheta_j^{n} - \beta_{j-\frac{1}{2}}\,\vartheta_{j-1}^{n} + \Delta t\,\epsilon_j^{n}$$

equation B.2 may be written as

$$A_j\,\vartheta_{j+1}^{n+1} + B_j\,\vartheta_j^{n+1} + C_j\,\vartheta_{j-1}^{n+1} = D_j \qquad j = 1, N \qquad \text{(B.3)}$$

which, when written for $j=1,N$ with the boundary conditions $\vartheta_0 = \vartheta_S$ at $z=0$ and $\vartheta_{N+1} = \vartheta_T$ at $z=h$, is a tridiagonal matrix equation which can be solved for the new values of the temperature, $\vartheta_1^{n+1}, \vartheta_2^{n+1}, \ldots, \vartheta_N^{n+1}$ by Richtmyer's "double sweep" method. From equation B.3 we see that we need values of ϑ_0 (when $j=1$) and ϑ_{N+1} (when $j=N$) in order to solve the system of equations. It is this, and not the physics of the problem, which requires the boundary conditions of section 2.4.

REFERENCES

Charney, J.G., 1973: in Dynamic Meteorology, P. Morel, ed. D. Reidel Publishing Co., Boston

Eady, E.T., 1949: Long waves and cyclone waves. Tellus, 1, No. 3, 33-52

Manabe, S. and R.F Strickler, 1964: Thermal equilibrium of the atmosphere with a convective adjustment. J. Atmos Sci, 21, 361-385

Manabe, S., and R.T. Weatherald, 1967: Thermal equilibrium of the atmosphere with a given distribution of relative humidity. J. Atmos Sci., 25, 241-259

Oort, A.H., and E.M. Rasmusson. 1971: Atmospheric Circulation Statistics NOAA Professional Paper 5

Pedlosky, J., 1970: Finite amplitude baroclinic waves. J. Atmos. Sci, 27, 15-30

Palmén, E., and C. W. Newton, 1969: Atmospheric Circulation Systems Academic Press, New York

Pond, S., G.T. Phelps, J.E. Paquin, G. McBean, and R.W. Stewart, 1971: Measurements of the turbulent fluxes of momentum, moisture, and sensible heat over the ocean. J. Atmos Sci, 28, 901-917

Richtmyer, R.D., and K. W. Morton, 1967: Difference Methods for Initial-Value Problems Interscience (John Wiley and Sons), New York

Stone, P.H., 1966: On non-geostrophic baroclinic stability J. Atmos. Sci., 23, 390-400

Stone, P.H., 1969: The meridional structure of baroclinic waves. J. Atmos. Sci., 26, 376-389

Stone, P.H., 1972a: On non-geostrophic baroclinic stability: Part III. The momentum and heat transports. J. Atmos. Sci., 29, 419-426

Stone, P.H., 1972b: A simplified radiative-dynamical model for the static stability of rotating atmospheres. J. Atmos. Sci., 29, 405-418

Taylor, R.J., 1956: Some measurements of heat flux at large negative Richardson number. Quart. J. Roy. Meteor. Soc., 81, 89-91

Yap, D., T.A. Black, and T.R. Oke, 1974: Calibration and test of a yaw-sphere thermometer system for sensible heat flux measurements. J. Appl. Meteor., 13, 40-45